Chapter 2

The heliosphere and cosmic rays

2.1 Introduction

In this and the following two chapters, the necessary background in order to understand long-term cosmic ray modulation in the heliosphere is discussed. Cosmic rays are energetic particles entering our heliosphere, the influential region of the Sun. They change their intensities as a function of position, energy and time, a process called the modulation of cosmic rays. This chapter starts with an overview on the Sun, its structure, composition and features. After this, a detailed discussion on the solar wind, heliospheric magnetic field (HMF), heliospheric current sheet (HCS) and the heliospheric structure is given. Lastly, cosmic rays, their composition and the various spacecraft which provide in-situ observations as used in this study are discussed. In the next chapter the focus shifts to the various transport coefficients.

2.2 The Sun

The Sun is our nearest star, at about 1 astronomical unit (AU) away from the Earth, and it is the source of energy for our planet. It is presently in a state of hydrostatic equilibrium where inward gravity (which causes a star to collapse) and outward pressure (which causes a star to expand) balance each other. The solar mass consists primarily of ∼90% hydrogen, ∼10% helium and elements like carbon, nitrogen and oxygen, which constitute about ∼0.1% (*Kivelson and Russel*, 1995). The Sun alone contains more than ∼99% of the total mass of the solar system and has an effective black body temperature of 5778 K. The radius of Sun, $r_{\odot}$, is about 696000 km (∼0.005 AU). See *Kivelson and Russel* (1995); *Stix* (2004); *Passos et al.* (2007); *Koskinen* (2011).

The Sun is not a perfect sphere; it is oblate as a result of solar rotation. The solar material consists mostly of ionised matter known as plasma. Due to this, the Sun has a differential rotation period which increases with the heliolatitude (angle above solar equatorial plane). It rotates faster at the equator (∼25 days) and slower towards the poles (∼36 days) (e.g. *Bartusiak*, 1994). Differential solar rotation occurs only in the convection zone of the Sun, while the radiative interior rotates almost rigidly (see *Fisk*, 1996; *Kuker and Stix*, 2001; *Balogh et al.*, 2008).

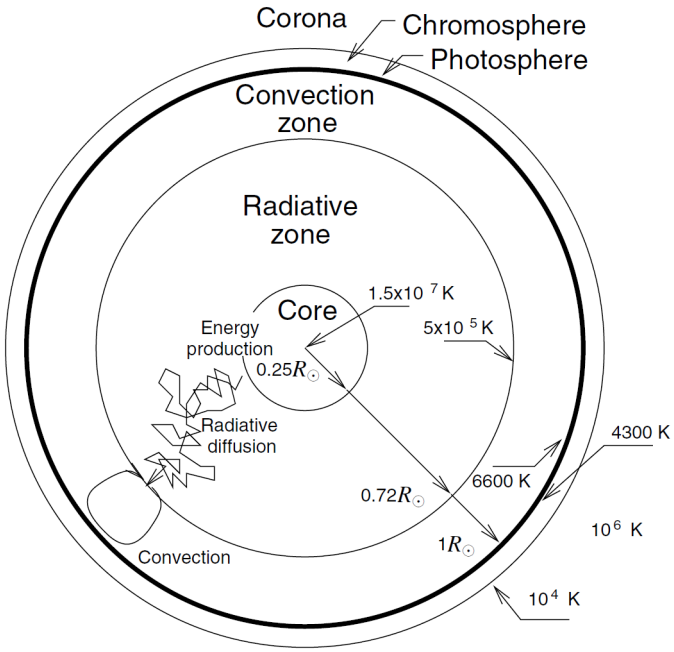

Figure 2.1: A graphical representation of the different regions of the Sun and their temperatures. From *Koskinen* (2011).

2.3 The structure of the Sun

The Sun can be divided mainly into six different regions: the core, the radiative zone, the convection zone, the photosphere, the chromosphere and the corona. Where the core, the radiative zone and the convection zone belong to the solar interior, the rest belongs to the solar surface and atmosphere. The solar interior is a region hidden from observation and the present accepted structure of the solar interior is based on theoretical solar models which make use of the global and surface features of the Sun. Figure 2.1 is a graphical representation of these different regions with their temperatures (see *Kivelson and Russel*, 1995; *Koskinen*, 2011).

2.3.1 The Core

The innermost region of the Sun is called the core. The core is the region where the Sun's energy production takes place through a thermonuclear fusion process in which hydrogen is consumed to form helium. The core has favourable temperature, density and pressure that is conducive to the fusion reaction process. More than 99% of the total energy generated in this fusion process is by the proton-proton (p-p) chain and the rest by the carbon-nitrogen-oxygen (CNO) cycle. The energy output leaves the solar surface as electromagnetic radiations. During this fusion of hydrogen to helium, elementary particles called neutrinos are formed and they escape the solar surface and can be detected on Earth. The core contains about half of the solar mass, although its radius is only one fourth of the solar radius (see e.g. *Castellani et al.*, 1997; *Brun et al.*, 1998; *Shaviv and Shaviv*, 2003; *Koskinen*, 2011).

2.3.2 The radiative zone

The core of the Sun is enclosed in a region called the radiative zone where the energy transfer mechanism is radiation. The energy produced in the core is transported outward towards the surface of the Sun through a very slow process of radiative diffusion of gamma rays (high energy photons) in the radiative zone. In this zone the photons are scattered, absorbed, and re-emitted over and over again by the dense solar matter, gradually making their way towards the solar surface. Due to this continuous scattering, absorption and re-emission, the initial wavelength of a photon generated in the core gets redshifted towards the visible wavelength, which is later emitted as sunlight. The radiative zone extents from $\sim 0.25 r_\odot$ up to $\sim 0.72 r_\odot$ (see *Eff-Darwich et al.*, 2002; *Turck-Chieze and Talon*, 2008; *Koskinen*, 2011).

2.3.3 The convection zone

The outermost region of the solar interior and the region above the radiative zone is called the convection zone. There is a thin transition layer between these two zones called the solar tachocline, where the HMF is probably created by the dynamo process (e.g. *Spiegel and Zahn*, 1992; *Brun et al.*, 1999). The radiative zone rotates rigidly while the convection zone experiences turbulent differential rotation like a fluid. The convection zone extends from $0.72 r_\odot$ to the surface of the Sun. Throughout this zone, energy is transferred to the solar surface by convection. In this region, the solar material is convectively unstable as compared to the radiation zone because the radial temperature gradients are larger.

The comparatively lower temperature in this zone makes the solar material opaque. As a result, it is difficult for photons to pass through. Due to this, energy is trapped in this zone making it more turbulent. By convective motion, the hot solar matter from the radiative zone rises up to the solar surface where it radiates photons and cools down, resulting in granulation which covers the surface of the Sun. Once cooled, the density of the matter increases and it falls back down through the edges of the granules to the top of the radiative zone. This process is continually repeated from the top of radiative zone to the solar surface (see e.g. *Garaud and Guervilly*, 2009; *Koskinen*, 2011).

2.3.4 The photosphere

The visible layer of the Sun is called the photosphere, and is often referred to as the surface of the Sun. This layer is the source of most of the heat and light that we receive on Earth. The thickness of the photosphere is about $\sim$500 km, which is a very thin region when compared to the solar radii. The temperature of the photosphere decreases with altitude, reaching minimum temperature at an altitude of about $\sim$500 km. The temperature at the bottom of the photosphere (which is in contact with the convection zone) is $\sim$6600 K and at the top the temperature is around $\sim$4300 K. Due to this temperature gradient, photons generated here are of

Figure 2.2: A photograph showing the corona of the Sun during solar maximum and minimum periods. The left image shows the appearance of corona during the total solar eclipse of 2001 when solar activity was maximal. The image at the right shows the same but during the total solar eclipse of 2009 when solar activity was minimal. Images from http://www.zam.fme.vutbr.cz/~druck/eclipse.

different wavelengths. The photosphere absorbs energy carried by convection and irradiates as a thermal black body at a temperature of ∼5778 K. Different features such as a sunspots, faculae, granules and supergranulation are observed on the photosphere (see *Robitaille*, 2006; *Koskinen*, 2011).

2.3.5 The chromosphere

The next layer is the chromosphere, where the temperature increases from ∼4300 K to nearly $\sim 10^4$ K. The reason behind this temperature increase in the chromosphere is not fully understood but believed to be due to the energy dissipation by the action of the solar magnetic field. This irregular layer is considered as the inner atmosphere of the Sun. The chromosphere cannot be seen by naked eye because the light from the photosphere overpowers its brightness. However, it can be observed as red in colour during solar eclipse. The thickness of this layer is around ∼2000 km. The temperature of the upper chromosphere increases rapidly to nearly ∼25000 K. The features of the chromosphere are filaments, prominences, spicules and flares (discussed later on). The chromosphere is followed by a very narrow transition layer where the temperature increases from $\sim 10^4$ K to $\sim 10^6$ K (see *Withbroe and Noyes*, 1977; *Pontieu et al.*, 2009; *Koskinen*, 2011).

2.3.6 The corona

The upper-most and the extended plasma atmosphere of the Sun is called the corona. The corona is a million times less bright than the photosphere. Due to this it can only be seen during total solar eclipse, when the solar disk is blocked by the Moon. It has an extremely high temperature ($\sim 10^6$ K) and less density. The increase in temperature to this value is also not fully understood. It is believed that magnetic fields are playing an active role in the solar

corona temperature increase by magnetic reconnection process. The corona extends into the interplanetary space and it becomes the solar wind.

The appearance of the corona depends on the solar activity cycle, which will be discussed later in Section 2.5. According to the appearance, the corona can be divided into three different areas which vary in size with solar activity: (1) active regions, (2) coronal holes and (3) quiet Sun. An active region represents the area of the corona with a strong magnetic field concentration which are visible as sunspots, faculae, flares, coronal mass ejections etc. This region is made up of closed magnetic field lines which form magnetic loops. Large closed magnetic loop structures are called helmet streamers, which connect regions of opposite magnetic polarity.

The coronal holes are dark regions seen in the corona where the magnetic field is not looped back to Sun and the magnetic field extends outward to form the interplanetary magnetic field, along which the solar plasma escapes into the interplanetary space. The coronal holes are the source of the fast solar wind. During solar minimum periods the coronal holes are mainly found at the polar regions of the Sun. However, during solar maximum periods they can be observed anywhere on the solar surface. The regions of the Sun not belonging to active regions and coronal holes are called the quiet Sun (see *Aschwanden*, 2005; *Cranmer*, 2009; *Wang*, 2009).

As mentioned above, the corona displays a variety of features including coronal holes and streamers. The images shown in Figure 2.2 shows how the overall appearance and brightness of the corona change with the solar activity cycle. The photo on left, which was taken during the total solar eclipse of 2001, shows the appearance of the solar corona when the solar activity was at maximum. During this period many streamers at all angles around the solar surface is visible. However, the image at the right was taken during the total solar eclipse of 2009 and when the solar activity was minimum. It shows how the appearance of the corona changed compared to the solar maxima. Only two large streamers are seen near the solar equator latitude during this period (see *Sime and Streete*, 1993; *Mikic et al.*, 2000; *Vourlidas*, 2006).

2.4 Features of the Sun

In this section different features of the Sun are discussed. The active regions of the Sun are the source of different solar features like sunspots, prominences, coronal mass ejections, flares, faculae, etc. The dynamics of this region change with time (every ∼11 years) leading to a period of maximum (more sunspots, coronal mass ejection, prominences, flares) and minimum (less of these features) solar activity periods. These different features of the Sun are illustrated in Figure 2.3.

Sunspots are visible dark areas of irregular shape on the surface of the Sun (photosphere). Temperatures in the dark central region, called the umbra, of sunspots is about ∼3700 K when compared to the surrounding solar surface temperature of ∼5778 K. The less darker surrounding region around the umbra is called penumbra. The left panel of Figure 2.3 with quadrant

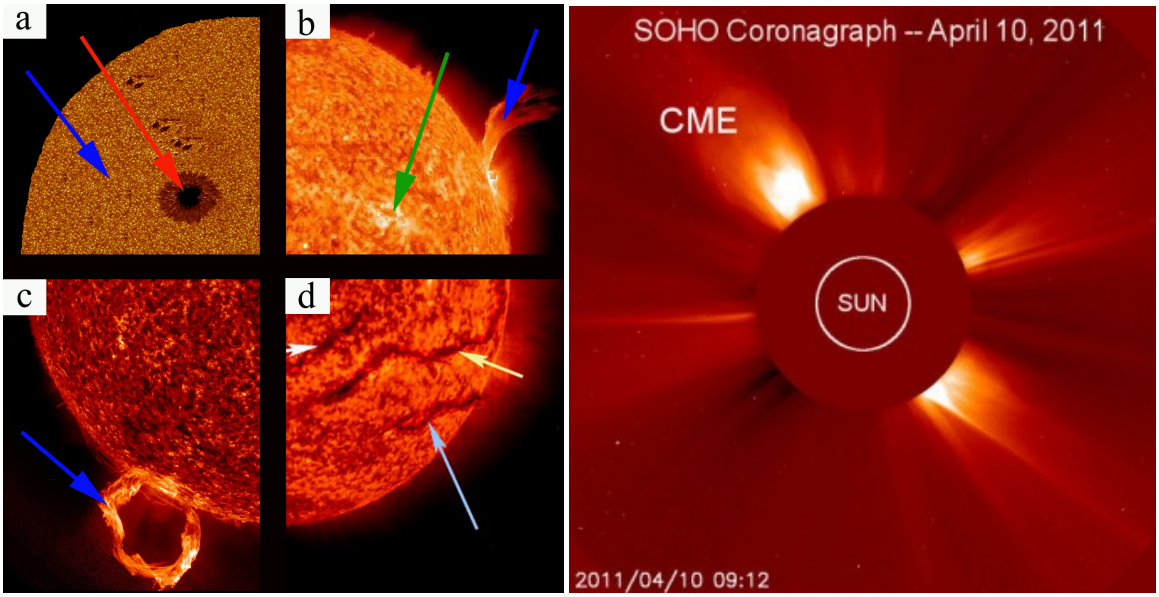

Figure 2.3: Images show different features observed on the Sun. On the left panel, quadrant (a) shows a sunspot with a red arrow and solar granules with a blue arrow. Quadrant (b) shows faculae with a green arrow and a solar flare with a blue arrow. Quadrant (c) shows a prominence and quadrant (d) shows filaments with pointed arrows. The right panel image shows a coronal mass ejection observed by SOHO spacecraft. Images from http://www.nasa.gov.

numbered (a) shows a sunspot with a red arrow, the dark umbra region and surrounding grey penumbra region can also be seen. The lifetime of a sunspot is typically several days, although larger ones may last for several weeks. The most full fledged sunspots have a penumbral diameter of $\sim$2-6$\times 10^4$ km.

Sunspots are magnetic regions on the Sun with magnetic field strengths of $\sim$0.3 T and field nearly vertical to the solar surface in the centre of the umbra. In the outer penumbra the field is $\sim$0.1 T and is nearly horizontal. Sunspots usually originate as a set of two sunspots. One sunspot will have positive or north magnetic field while the other one will have negative or south magnetic field (see e.g. *Moore and Rabin*, 1985; *Baumann and Solanki*, 2005).

After sunspots, faculae are the next obvious feature on the solar disk. Faculae have been known since telescopes have been pointed at the Sun. Faculae appear as bright areas that are usually most easily seen near the limb, or edge, of the solar disk but invisible at the centre. The left panel of Figure 2.3 with quadrant numbered (b) shows a faculae with a green arrow. Like sunspots, faculaes are also magnetic areas but the magnetic field is concentrated in much smaller bundles compared to sunspots. However, faculae are brighter when compared to the sunspots which are darker. The brightness of the faculae dominate the darker sunspots making the Sun appear slightly brighter during solar maximum compared to solar minimum (*Dicke*, 1970; *Keller et al.*, 2004).

Cellular features of about $\sim$1000 km across and with a lifetime of about $\sim$10-20 minutes, which are observed on the solar surface (excluding the area covered by the sunspots), are called gran-

ules. They look similar to bubbles on the surface of boiling water. The cellular pattern of the granules are due to the convective motion of the solar material. The hot plasma rises up from the solar interior to the bright area of granules, it then spread out across the surface and later sinks to the solar interior along the dark lanes giving rise to a cellular pattern with a dark perimeter and bright centre. The granules are continually evolving as old granules are pushed aside by newly emerging ones. The left panel of Figure 2.3 with quadrant numbered (a) shows granulation on the solar surface as indicated by the pointed blue arrow. Granules which are $\sim$25 times larger are called supergranules. They are $\sim$35000 km across and has a lifetime of $\sim$1-2 days. These features also cover the entire Sun and are continually evolving (*Leighton*, 1963; *Nelson and Musman*, 1978; *DeRosa and Toomre*, 2004).

An arch-like large magnetic structure confining a cool (temperature $\lesssim 10^4$ K) and dense plasma in the hot solar corona is called a filament or a prominence. This structure is called a filament when seen against the solar disk, which appears as a dark feature in the bright solar disk background, and is called a prominence when seen above the solar limb which appears brighter in the dark background around the Sun. The prominence or filament plasma is $\sim$100 times cooler and denser than its coronal surroundings. The left panel of Figure 2.3 with quadrant numbered (c) shows a prominence and quadrant numbered (d) shows filaments as indicated by the pointed arrows. Prominences are divided into two groups namely quiescent prominences and active prominences. The quiescent prominences are relatively stable features lying outside active regions with lifetimes ranging from a few days up to several months. Their dimensions are in the range of a few $10^4 - 10^5$ km in length, and a few $10^3 - 10^4$ km thick and the heights are of the order of $10^4 - 10^5$ km. However, the active prominences are dynamical features typically occurring in the vicinity of active regions with a height which is smaller than that of quiescent prominences and are usually short-lived with a lifetime which is smaller than the lifetime of the associated active region (*Labrosse et al.*, 2010; *Mackay et al.*, 2010).

The most powerful magnetic events on the Sun which can release $\sim 10^{25}$ J of energy on a time scale of several tens of seconds to several tens of minutes are called flares. They are actually explosively erupting prominences. The left panel of Figure 2.3 with quadrant numbered (b) shows a flare as indicated by the pointed blue arrow. The flares emit radiation across the entire electromagnetic spectrum, from radio to gamma rays. They are also associated with the acceleration of particles and coronal mass ejections. The flares are the result of the rapid release of energy previously stored as inductive magnetic fields due to electrical currents flowing into the corona. Flares can be divided into two classes namely impulsive and gradual. Gradual events are large flares which occur high in the corona and which produce long-duration soft and hard X-rays and gamma rays. However, impulsive events are more compact flares which occur on the lower corona and produce short duration radiations (*Miller*, 1998; *Fletcher et al.*, 2011; *Hudson*, 2011).

Huge clouds of plasma which erupt from the Sun's corona are called coronal mass ejections (CMEs). The right panel of Figure 2.3 shows a CME observed by the SOHO spacecraft. These

structures appear as bright loops moving away from the Sun. CMEs usually come from active regions in close association with major solar flares, but they also can come from filament channels in the quiet Sun. CMEs associated with active regions have higher average speeds than CMEs associated with eruptive prominences located away from active regions. CMEs occur on a time scale of few minutes to several hours. They are responsible for the removal of magnetic helicity[1] and large quantity of mass ($\sim 10^{12} - 10^{13}$ kg) from the solar corona. CMEs drive shocks from close to the Sun to far into the interplanetary medium, the shocks being the strongest near the Sun. CME driven shocks accelerate charged particles from close to the Sun and in the interplanetary medium. When they move further into interplanetary space they become interplanetary coronal mass ejections (ICMEs) which are responsible for severe geomagnetic storms observed at Earth (*Gopalswamy*, 2006; *Hudson et al.*, 2006; *Howard and Tappin*, 2009).

2.5 Solar activity cycle

Sunspots are a measure of solar activity and have been observed systematically for hundreds of years. Galileo in 1612 noted that sunspots seemed to be moving on the solar surface and he interpreted that this was because the Sun is rotating with a rotation period of ∼27 days, slightly faster at the equator as compared to higher latitudes. The solar activity cycle is assumed to be the result of the solar differential rotation and the related internal solar dynamo (*Babcock*, 1961; *Schwadron et al.*, 2008). The number of sunspots seen on the solar surface changes from year to year. This increase and decrease in sunspot counts is a cycle which repeats every ∼11 years on average. A peak in the sunspot count is called a solar maximum period and the time when few sunspots appear is called a solar minimum period.

Sunspot numbers form the longest directly observed index of solar activity since 1610 (*Hoyt and Schatten*, 1998). Figure 2.4 shows the monthly averaged International Sunspot Numbers (Wolf or Zurich sunspot numbers) from 1750 to 2011. Officially the first solar cycle started in 1755, shown in the figure with a red circle, and the last cycle (23^{rd}) ended on December 2008, at present, solar cycle number 24 is in progress (*Usoskin et al.*, 2001; *Ahluwalia and Ygbuhay*, 2009; *Kane*, 2011).

The Royal Greenwich Observatory has been providing a detailed sunspots record since 1874, which include the sunspot number and information of the area and position of each sunspot. It is found that sunspots do not appear randomly on the solar surface but are concentrated in two latitude bands on either side of the solar equator. Figure 2.5 shows the area and position of each sunspot during each solar rotation since 1874. The top panel of the figure shows the areas of sunspots as a function of latitude and time. Sunspots first form at mid-latitudes, around $\sim 30^o$-45^o and later move towards the solar equator. When these sunspots fade, sunspots of

[1] Magnetic helicity is a quantity that describes solar magnetic field topology like the helically twisted, sheared, inter-linked and braided magnetic field lines (*Lynch et al.*, 2005).

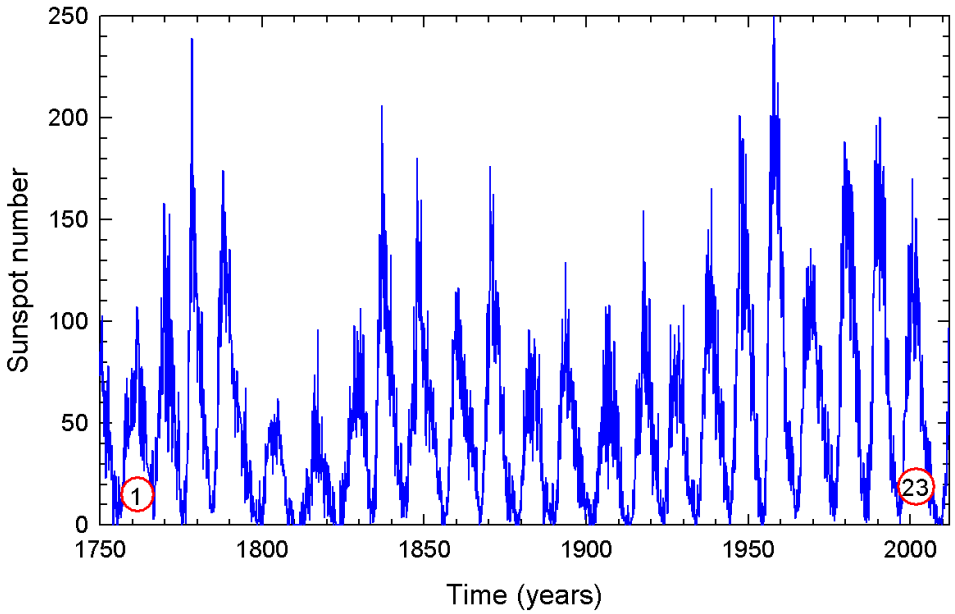

Figure 2.4: Monthly averaged sunspot numbers from 1750 to 2011. The red circled 1 and 23 denote the first official solar cycle and the last (23^{rd}) solar cycle which ended on December 2008. Data from: ftp://ftp.ngdc.noaa.gov.

the new cycle start appearing at mid-latitudes. This pattern looks similar to a butterfly and is called the Maunder Butterfly diagram (*Maunder*, 1904). The lower panel of the figure shows the observed area of sunspots represented in terms of percentage area of visible hemisphere for each solar rotation (*Hathaway et al.*, 2003; *Ternullo*, 2007; *Arlt*, 2009).

The observations by *Hale and Nicholson* (1925) revealed that apart from the ∼11 year solar (sunspot) cycle, the Sun also exhibits a ∼22 year magnetic cycle called the Hale cycle (*Babcock*, 1961; *Leighton*, 1969). The magnetic fields on the Sun were first observed in sunspots by *Hale* (1908). When the sunspots come in pairs on the solar surface, each sunspot in this pair has a magnetic polarity opposite to that of its pair, similar to the ends of a bar magnet. In the northern hemisphere of the Sun during a given sunspot cycle, all the leading sunspots (with respect to the direction of the solar rotation) in the groups tend to have the same polarity. During the same period all the leading sunspots in the southern hemisphere also tend to have same polarity but their polarity is just opposite to what is observed in the northern hemisphere. Figure 2.6 shows this phenomenon during solar cycle 22 and 23 with yellow colour denoting magnetic north polarity and blue denoting magnetic south polarity. The figure on the left shows a magnetogram during solar cycle 22 on the 2^{nd} August 1989, for which the leading sunspot distribution in the northern hemisphere has a magnetic south polarity (blue) and in the southern hemisphere the leading sunspots are observed to be having magnetic north polarity (yellow). However, during solar cycle 23 on the 26^{th} June 2000, the right panel figure shows that the polarity of the leading sunspots are reversed with yellow leading in the northern hemisphere and blue leading in the southern hemisphere. This observed reversal of polarity in each hemi-

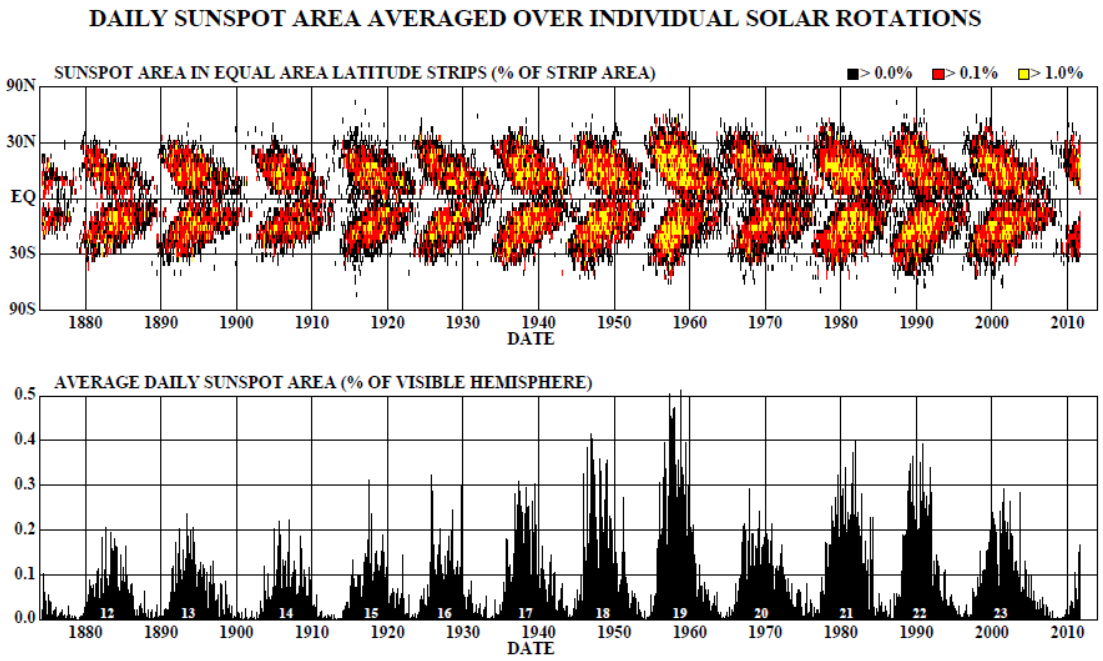

Figure 2.5: Top panel shows a butterfly diagram illustrating the distribution of sunspots in latitude at different times. Lower panel shows the average daily sunspot area as percentage of the visible hemisphere at different times. From http://solarscience.msfc.nasa.gov.

sphere with solar cycle is called Hale's polarity law (*Hathaway*, 2010).

Similar to the sunspot butterfly diagram, magnetogram observations revealed a magnetic butterfly diagram which illustrate Hale's polarity law and ∼22 year Hale cycle. Figure 2.7 shows a magnetic butterfly diagram where the magnetic flux positions are plotted as a function of time and latitude. The radial magnetic field which is averaged over longitude for each solar rotation obtained from the instruments on Kitt Peak National observatory and SOHO spacecraft is used by *Hathaway* (2010) to construct the magnetic butterfly diagram as shown in Figure 2.7. The colour yellow and blue in Figure 2.7 denote the same as in Figure 2.6. From the Figure 2.7, it follows that the polarity of the each hemisphere reverses every ∼11 years and the polarity in each hemisphere is opposite to each other. In addition to that, at high latitudes a motion of magnetic flux towards the polar regions are observed. Also a cycle which repeats ∼22 years, the Hale cycle is evident. The last Hale cycle was composed of solar cycle 22 and 23. The ∼22 solar cycle will be again discussed later in Section 2.11 from a cosmic ray perspective.

2.6 The solar wind

The solar wind is a continuous radial outflow of solar material from the Sun. The existence of such a wind came from the study of *Biermann* (1951, 1957) about comet tail orientation. He determined that the plasma tail or ion tail which always point radially away from the Sun is due to the radially expanding solar wind. However, the dust tail that curves away

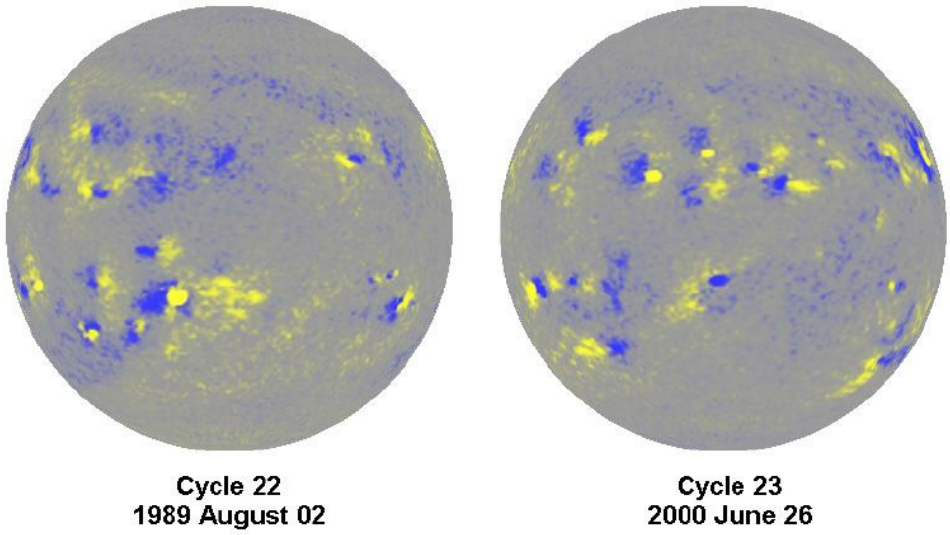

Figure 2.6: Magnetograms taken during solar cycle 22 on 2^{nd} August 1989 (left) and solar cycle 23 on 26^{th} June 2000 (right). The yellow colour denote magnetic north (positive) polarity and blue denote magnetic south (negative) polarity. The leading sunspots in one hemisphere have opposite magnetic polarity to those in the other hemisphere. In left panel the blue (south polarity) is leading in northern hemisphere and yellow (north polarity) leading in the southern hemisphere. The right panel shows that the polarity reverses from one cycle to the next. From *Hathaway* (2010).

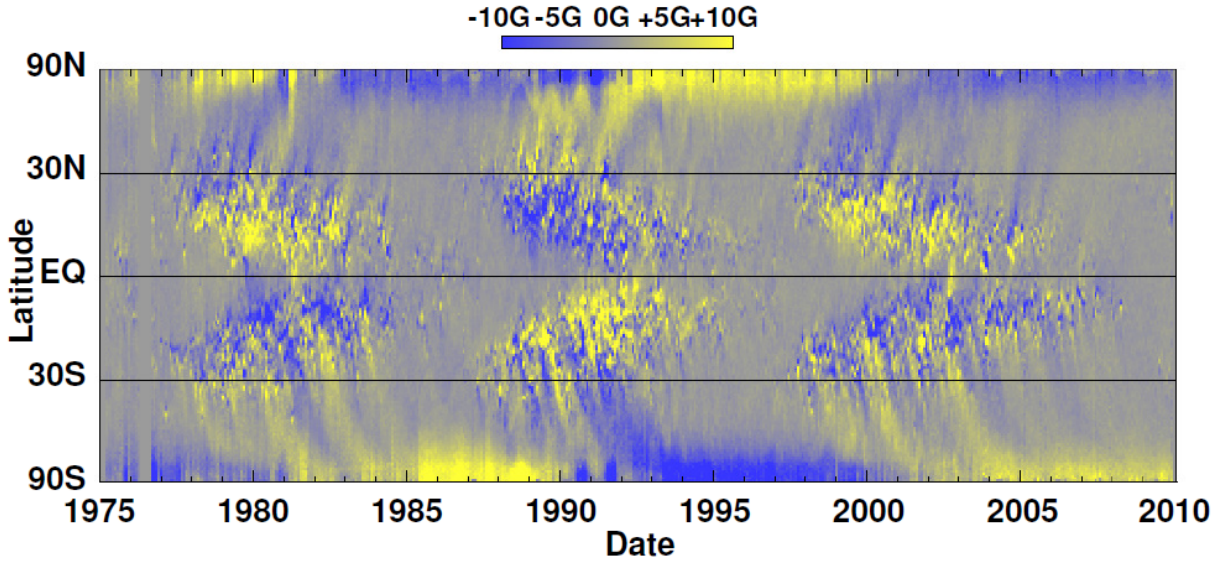

Figure 2.7: A magnetic butterfly diagram constructed using the radial magnetic field which is averaged over longitude for each solar rotation obtained from the instruments on Kitt Peak National observatory and SOHO spacecraft. The colour yellow and blue denotes the same as in Figure 2.6. From *Hathaway* (2010).

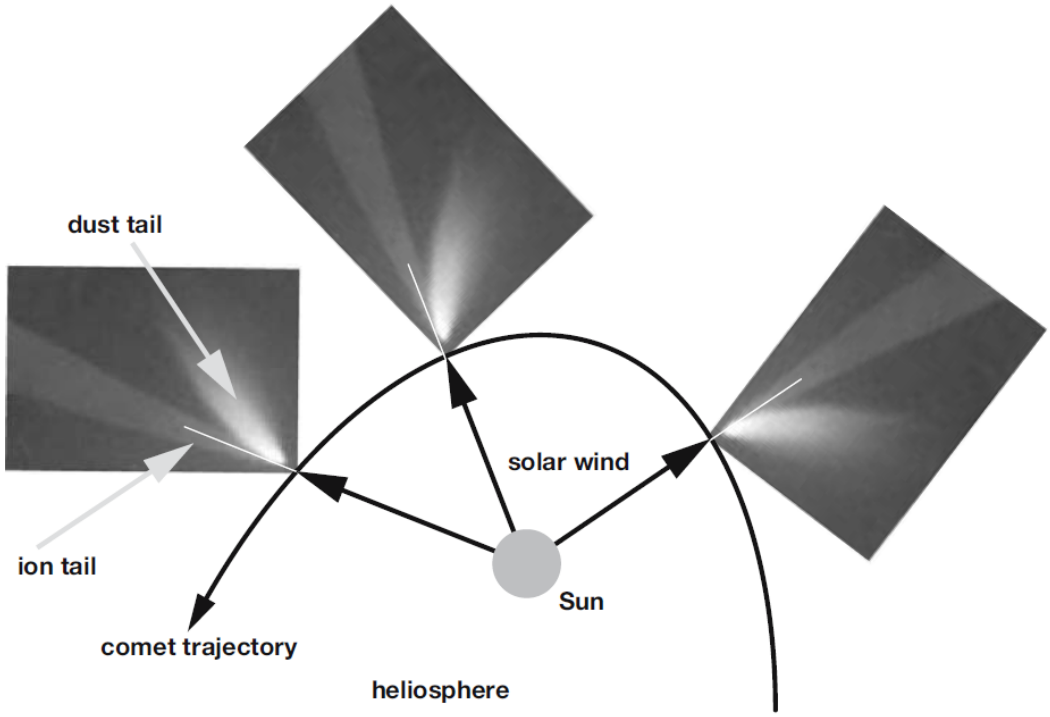

Figure 2.8: A graphical representation of a comet's trajectory showing its ion tail which is always pointed radially away from the Sun and the dust tail which curves away from the comet. From *Balogh et al.* (2008).

from the comet is due to the solar radiation pressure (sun light) which strike the dust particles that flow out from the comet. A graphical representation of a comet's trajectory and both its tails are shown in Figure 2.8. The solar wind was first called solar corpuscular radiation and later the name solar wind was introduced by *Parker* (1958) who predicted the solar wind as a supersonic flow of plasma in interplanetary space. The supersonic solar wind as predicted was later confirmed by in-situ observations by different spacecraft.

The source of the solar wind is the Sun's corona where the temperature is as high as $\sim 10^6$ K. This high temperature makes the Sun's gravitational force inadequate to hold on to the solar particles, and as a result of this the Sun is continuously blowing away its atmosphere to maintain equilibrium (*Parker*, 1958). The solar wind is composed of ions (mainly ionised hydrogen (protons), a small percentage of fully ionised helium (alpha particles) and the rest with fully or partially ionised heavier elements such as carbon, oxygen, silicon, magnesium, iron etc) and the electrons these ions have lost (*Bochsler*, 2008). At the orbit of Earth, the solar wind has an average density of $\sim$7 particles.cm^{-3} and has a velocity that varies from $\sim$250 km.s^{-1} to $\sim$1000 km.s^{-1} depending on the solar region from which it was emitted and the phase of the solar cycle (*Balogh et al.*, 2008).

Ulysses, the first spacecraft to explore and take measurements over the polar regions of the Sun, established that the solar wind velocity is not uniform at all latitudes. The Ulysses trajectory is shown later in Figure 2.27. From measurements on-board this spacecraft it follows that the solar wind can be divided into a slow and a fast solar wind. The Sun's magnetic field is the

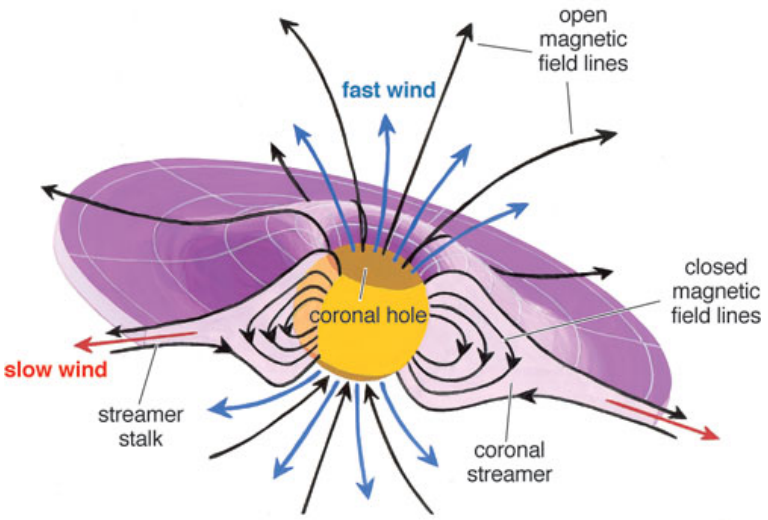

Figure 2.9: A graphical representation of the origin of fast and slow solar wind. The fast wind (blue) blows out from the coronal holes along open magnetic field lines while the slow wind (red) emanates from the stalks of the coronal streamers, above the closed magnetic field lines. From http://www.americanscientist.org.

main cause of the difference between the slow and the fast solar wind. At lower solar latitudes during solar minimum periods, the Sun's magnetic field forms loops which begin and end on the solar surface. These loops stretch away to form the streamer belts. The middle regions of these streamer belts are parallel to the solar surface and are perpendicular to the radially outflowing solar wind. The magnetic field, which are perpendicular to the solar wind, prevent it from escaping, and these streamer belts are regarded as prime candidates causing the slow solar wind speed. Slow solar wind also arise from the small coronal holes and also from the edges of large coronal holes (*Ofman*, 2004; *Schwenn*, 2006; *Wang*, 2011).

The coronal holes, low density regions in the corona, are the source of the fast solar wind. They are located in the polar regions of the Sun during solar minimum periods. Open field lines extend from the coronal holes towards the interplanetary space and these field lines have only one end attached to the solar surface. The open field lines assist the radial outflow and the fast solar wind evolves from this region (see *Cranmer*, 2009; *Wang*, 2009). These open magnetic field lines contribute to the cosmic ray modulation in the heliosphere.

The slow speed solar wind as measured at Earth's orbit and beyond is characterised by its velocity of $\sim$400 km.s^{-1} and by its frozen-in temperature of $\sim$1.4-1.6 $\times 10^6$ K. However, the fast speed solar wind is characterised by its velocity of $\sim$750 km.s^{-1} and its frozen-in temperature of $\sim 8 \times 10^5$ K (*Feldman et al.*, 2005). A graphical representation of the origin of the fast and slow solar wind is shown in Figure 2.9. The figure shows the coronal hole regions where open magnetic fields are found, which are responsible for the fast solar wind (blue) while the streamers found above the closed magnetic fields is responsible for the slow solar wind (red).

The latitudinal dependence of the solar wind speed as observed by Ulysses during two solar

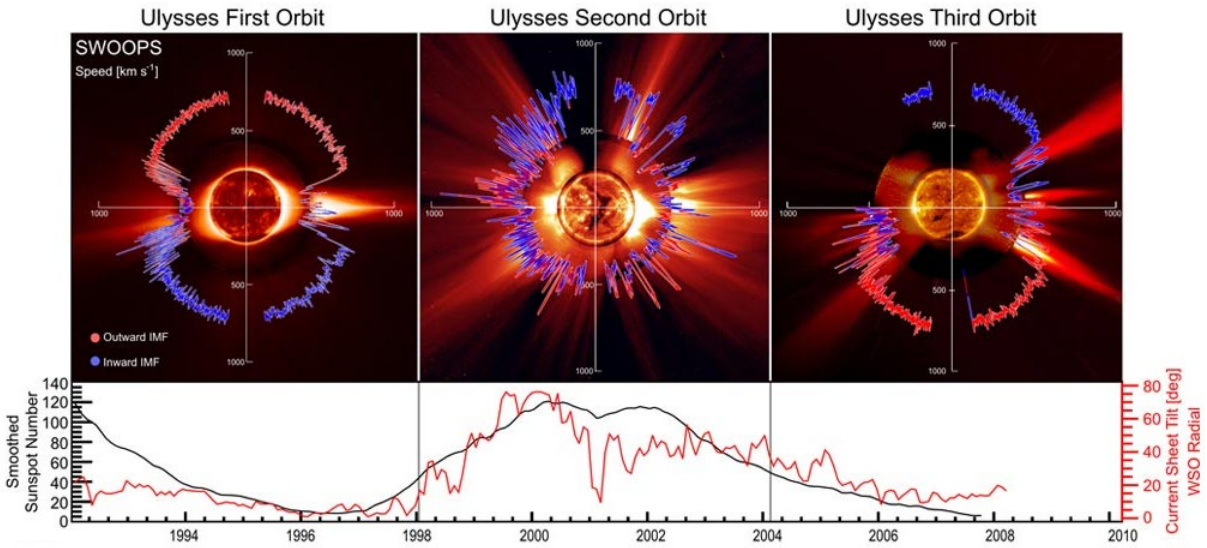

Figure 2.10: The upper panel shows polar plots of the solar wind speed during the three out-of-ecliptic orbits of the Ulysses spacecraft. The measured magnetic field polarity is indicated by blue and red colour. Overlaid are images from the Solar and Heliospheric Observatory (SOHO) spacecraft. The lower panel shows the smoothed sunspot number (black) and HCS tilt angle (red) as a function of time, lined up to match the period for each out-of-ecliptic orbit of Ulysses. From *McComas et al.* (2008).

minimum and a maximum period is shown in Figure 2.10. The upper panel of figure shows polar plots of the solar wind speed during the three out-of-ecliptic orbits of Ulysses. The magnetic field polarity measured by Ulysses is indicated by blue and red colour. Overlaid are images from the Solar and Heliospheric Observatory (SOHO) spacecraft. The lower panel shows the smoothed sunspot number (black) and HCS tilt angle (red) as a function of time, lined up to match the period for each out-of-ecliptic orbit of Ulysses. The left and right polar plot in the upper panel shows the solar wind speed during solar minimum period where the streamers are seen in the low latitude regions. These polar plots look very similar except the HMF polarity is reversed. During this period the solar wind speed was measured to be non uniform, from high to low latitudes. The speed changes from $\sim$800 km.s^{-1} above the coronal holes to $\sim$300-400 km.s^{-1} above the streamer belt. During the solar minimum period, the solar wind speed at high latitudes is measured to be almost uniformly fast but a solar wind of varying speed is measured at the lower latitude. However, during solar maximum period (polar plot shown in the middle of the upper panel) a complicated highly variable solar wind speed profile is measured for all heliolatitudes. The low speed solar wind regions (streamers) are observed to also extend to higher latitudes during this period of increased solar activity. (*Fujiki et al.*, 2003; *McComas et al.*, 2008; *Heber*, 2011).

Besides the latitude dependence in solar wind speed there is also a remarkable radial dependence close to the Sun. Figure 2.11 shows a compilation of speed profiles from various observations and models of the fast solar wind by *Esser et al.* (1997). The solar wind speed is shown as a function of $r/r_\odot$ with $r_\odot$ the solar radius ($20r_\odot \approx 0.1$ AU). Dotted horizontal lines

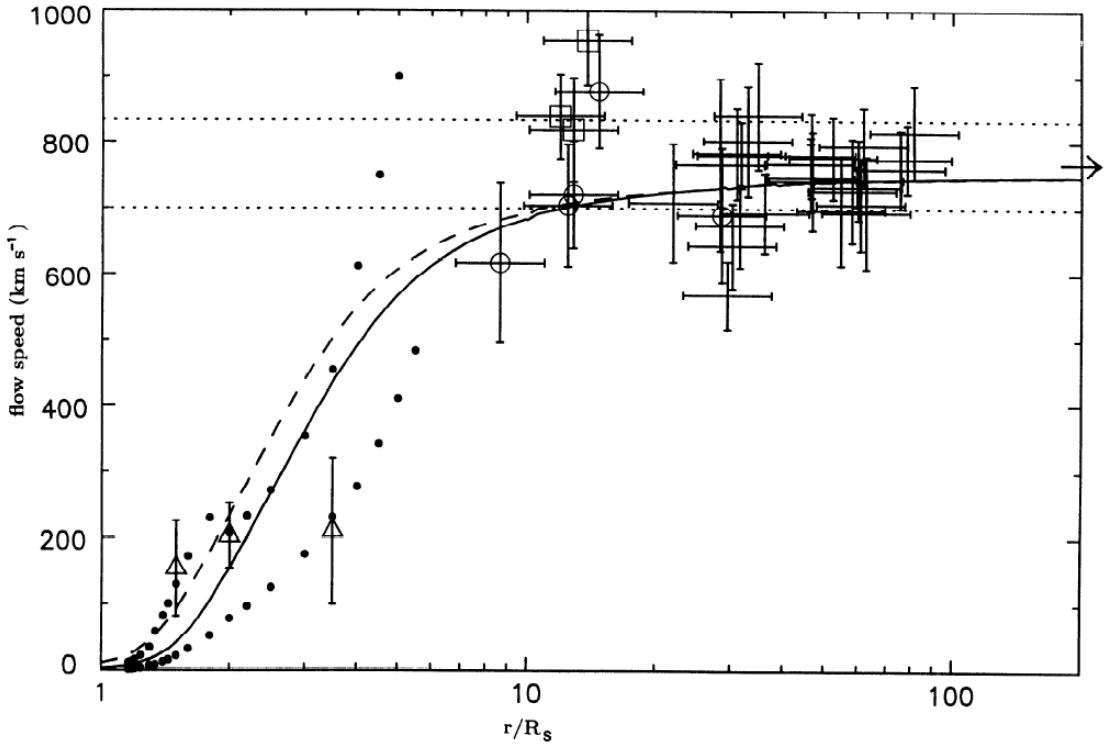

Figure 2.11: Speed profiles of the fast solar wind measured by various spacecraft and model results as a function of $r/r_\odot$ with $r_\odot$ the solar radius ($20r_\odot \approx 0.1$ AU). Dotted horizontal lines shows the range of flow speeds measured by Ulysses in high speed wind at high latitudes. The solid and dashed lines are the two flow speeds calculated by *Esser et al.* (1997). Note that R_s in the figure denotes $r_\odot$. From *Esser et al.* (1997).

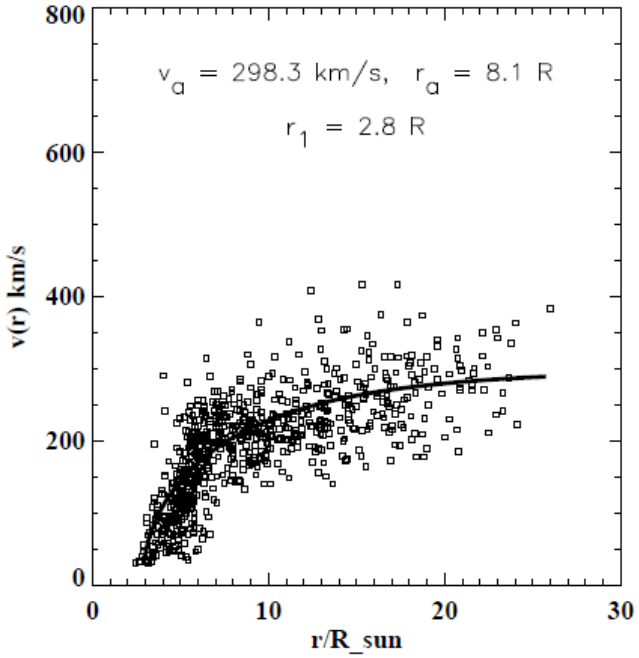

Figure 2.12: Speed for 65 individual moving density enhancements in the slow solar wind stream as a function of $r/r_\odot$. The figure shows that the speed of these enhancements tends to cluster along a quasi-parabolic path. The solid line is the best fit to the data points. Note that R_sun in the figure denotes $r_\odot$. From *Sheeley et al.* (1997).

show the range of flow speeds measured by Ulysses in the high speed wind at high latitudes. The solid and dashed lines are the two flow speeds calculated by *Esser et al.* (1997). The figure shows that the solar wind is accelerated to 50% of its speed by $4r_\odot$ and to 90% by $30r_\odot$.

The slow solar wind increases less rapidly as a function of increasing distance compared to the fast solar wind. Figure 2.12 shows the speed for 65 individual moving density enhancements in the slow solar wind stream as a function of $r/r_\odot$. The figure shows that the speed of these enhancements tends to cluster along a quasi-parabolic path. The solid line is the best fit to the data points computed by *Sheeley et al.* (1997). The slow solar wind begins to accelerate from a distance around $3r_\odot$, by $10r_\odot$ they reach a speed of around $\sim$200 km.s^{-1} and $\sim$300 km.s^{-1} at $30r_\odot$. This speed profile is fairly consistent with an isothermal expansion at a temperature of 1.1×10^6 K and is in good agreement with the solar wind model by *Parker* (1958). It also fits well to the in-situ measurements from Helios at $60r_\odot$ of $\sim$350 km.s^{-1} (*Schwenn*, 2006). The radial dependence of solar wind shows that both the slow and fast solar wind are accelerated within 0.1 AU and become a steady flow at around 0.3 AU (*Esser et al.*, 1997; *Sheeley et al.*, 1997; *Kojima et al.*, 2004; *Ashbourn and Woods*, 2005).

To model the solar wind velocity $\mathbf{V}$ in modulation models (*Ferreira*, 2002; *Langner*, 2004; *Strauss*, 2010), a latitude and radial dependence is incorporated into the radially outflowing solar wind. These latitudinal and radial dependencies are assumed to be independent of each other and is given as (*Hattingh*, 1998),

$$\mathbf{V}(r,\theta) = V(r,\theta)\mathbf{e}_r = V_r(r)V_\theta(\theta)\mathbf{e}_r, \tag{2.1}$$

where r is the radial distance in AU, θ the polar angle (angle measured from the Sun's North pole) and $\mathbf{e}_r$ the unit vector in the radial direction. Note that Equation 2.1 is not valid inside 0.3 AU and outside the termination shock.

For the latitude dependence $V_\theta(\theta)$ of the solar wind velocity during solar minimum conditions, the latitudinal solar wind profile constructed by (*Hattingh*, 1998) is used in this work and is given as,

$$V_\theta(\theta) = 1.5 \mp 0.5\tanh\left[\frac{2\pi}{45}(\theta - 90^o \pm \varphi)\right], \tag{2.2}$$

where $0^o \leq \theta \leq 90^o$, the northern hemisphere and $90^o \leq \theta \leq 180^o$, the southern hemisphere respectively with $\varphi = 30^o$. The φ determines at which polar angle the solar wind speed must start to increase from 400 km.s^{-1} to 800 km.s^{-1}.

During solar maximum conditions no latitudinal dependence is observed, so it is assumed as,

$$V_\theta(\theta) = 1.0. \tag{2.3}$$

The latitude dependence of the solar wind speed as modelled using Equations 2.2 (solar minima) and 2.3 (solar maxima) is shown in Figure 2.13 as a function of θ. The modelled speed profiles for solar minima and maxima are compared with the Ulysses measurements during the three fast latitude scan (FLS) periods, represented in the figure as FLS1 (grey line), FLS2

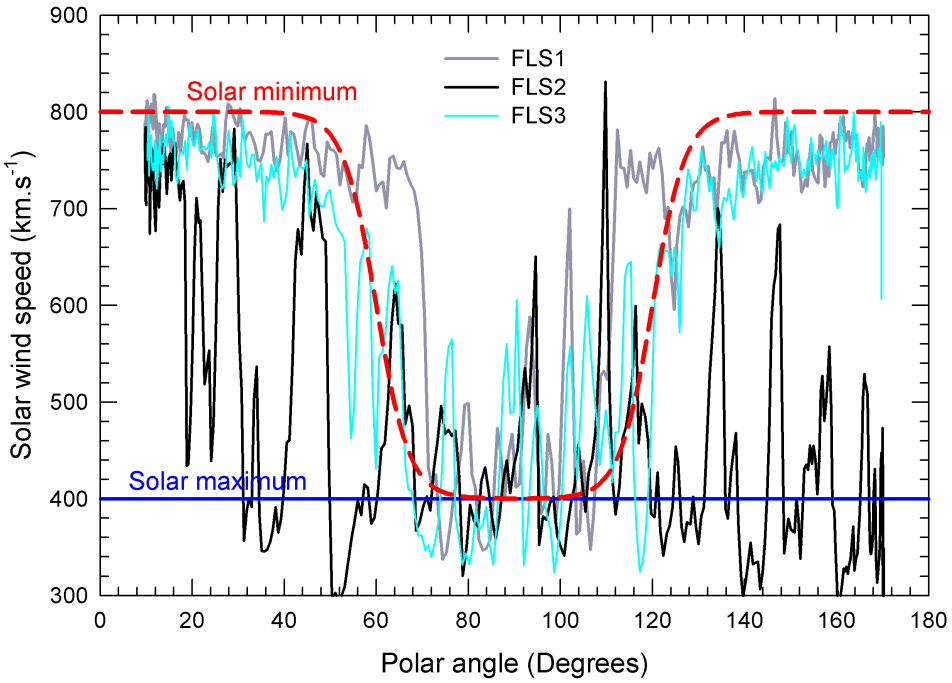

Figure 2.13: The latitude dependence of the solar wind speed as a function of polar angle θ during solar minima (dashed red line representing Equation 2.2) and maxima (solid blue line representing Equation 2.3). The modelled solar wind profile is compared with the Ulysses solar wind speed measurements during the three fast latitude scans (FLS), as given by FLS1, FLS2 and FLS3. The FLS1 (grey line) and FLS3 (cyan line) was during solar minimum periods but the FLS2 (black line) was during a solar maximum period. Data from: http://cohoweb.gsfc.nasa.gov.

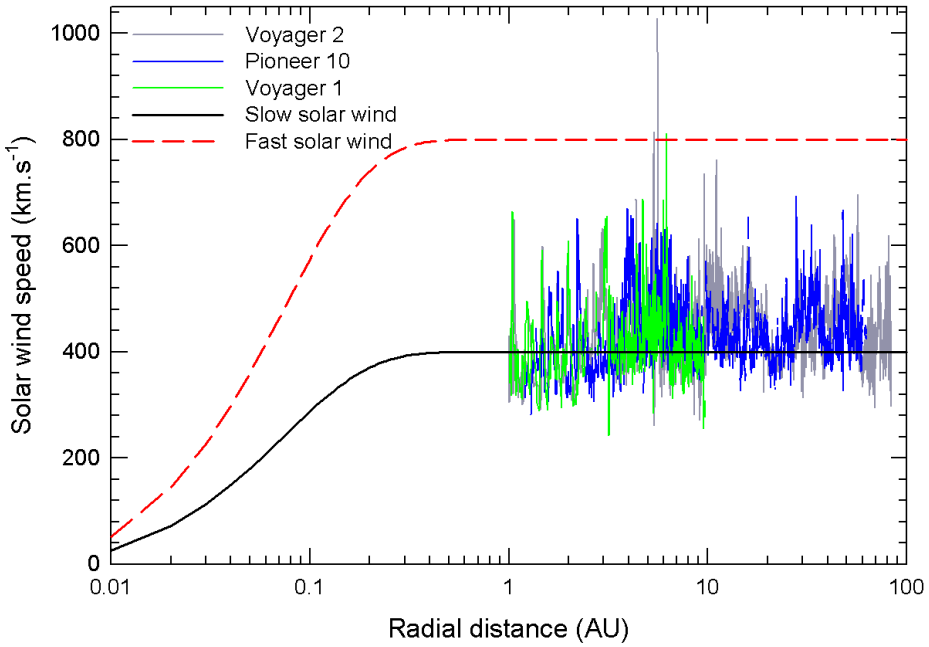

Figure 2.14: The radial dependence of the solar wind speed as modelled in this study is shown as a function of radial distance from the Sun. The modelled fast solar wind (red dashed line) and slow solar wind (black solid line) are compared with solar wind measurements from the spacecraft Pioneer 10 (blue), Voyager 1 (green) and Voyager 2 (grey). Note that these spacecraft are in the equatorial regions therefore not observing the fast solar wind speed. Data from: http://cohoweb.gsfc.nasa.gov.

(black line) and FLS3 (cyan line). FLS1 and FLS3 occurred during solar minimum conditions but FLS2 occurred during a solar maximum activity period. Concerning the model, the red dashed line (Equation 2.2) shows that $V = 800$ km.s^{-1} in the fast solar wind region ($\sim 40^o$ near poles) and $V = 400$ km.s^{-1} in the slow solar wind region ($\sim 10^o$ near equatorial plane) during a solar minimum period. However, during solar maximum period $V = 400$ km.s^{-1} for all θ as shown by the blue solid line. When compared to the Ulysses observations, the solar wind speed profiles assumed in the model during solar minima and maxima are largely compatible with the observations.

The radial dependence $V_r(r)$ of the solar wind inside the termination shock is given as (*Hattingh*, 1998),

$$V_r(r) = V_o \left(1 - \exp\left[\frac{40}{3}\frac{(r_\odot - r)}{r_o}\right]\right), \tag{2.4}$$

with $r_o = 1$ AU, $V_o = 400$ km.s^{-1} and $r_\odot = 0.005$ AU. After the shock, the radial solar wind speed decreases according to the compression ratio and then decreases as r^{-2} further in the inner heliosheath to the heliopause (*Strauss*, 2010).

The radial dependence of both the fast and slow solar wind is shown in Figure 2.14. The modelled radial solar wind profile is compared with the solar wind measurements taken by different spacecraft namely, Pioneer 10, Voyager 1 and Voyager 2 (from `http://cohoweb.gsfc.nasa.gov`). The modelled fast (red dashed line) and slow (black solid line) solar wind stream profiles show that they are accelerated very rapidly to a constant speed at ~0.3 AU away from the Sun (see e.g. *Esser et al.*, 1997; *Sheeley et al.*, 1997; *Kojima et al.*, 2004; *Ashbourn and Woods*, 2005; *Schwenn*, 2006). The spacecraft Pioneer 10, Voyager 1 and Voyager 2 all stayed within $\sim 35^o$ close to the equatorial plane in the slow solar wind stream while it moved into the outer heliosphere therefore not observing the fast solar wind stream. The Voyager trajectory is later shown in Figure 2.29. When compared to spacecraft measurements, the radial dependence modelled by Equation 2.4 (e.g. *Hattingh*, 1998; *Ferreira*, 2002; *Langner*, 2004; *Strauss*, 2010) resulted in a realistic solar wind profile.

2.7 The heliospheric magnetic field

The magnetic field of the solar corona, which is frozen into the solar wind, is carried by the solar wind into the interplanetary space where it is called the Interplanetary Magnetic Field (IMF) or the Heliospheric Magnetic Field (HMF). The Sun's magnetic field becomes approximately radial at a heliocentric distance of ~2.5$r_\odot$ called the source surface (*Wang and Sheeley*, 1995; *Lockwood and Stamper*, 1999). Below the source surface the coronal material is controlled by the Sun's magnetic field. However, after $\sim 20r_\odot$ the solar wind completely dominates the flow (*Schatten et al.*, 1969). The HMF is a weak magnetic field compared to other astrophysical bodies, but it extends over the whole heliosphere and modulates cosmic rays as well as solar particles.

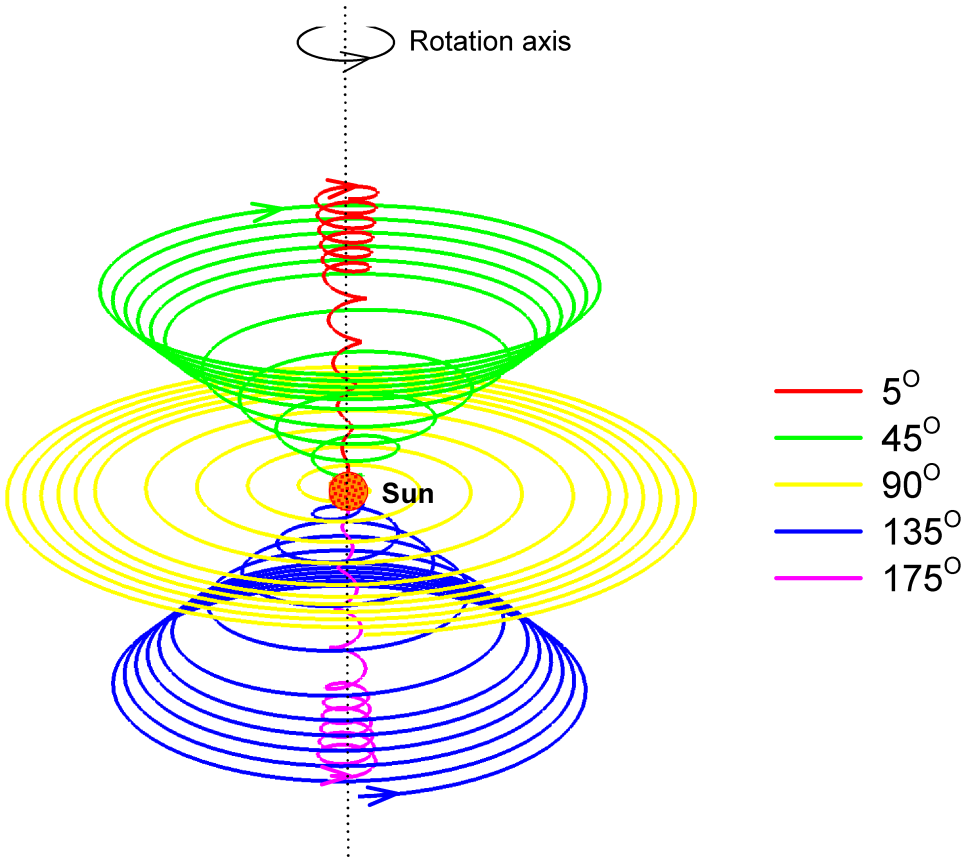

Figure 2.15: A graphical illustration of the 3D structure of the HMF (Parker field) lines corresponding to different polar angles 5^o (red), 45^o (green), 90^o (yellow), 135^o (blue) and 175^o (purple) with Sun at the centre. The magnetic field lines are compressed from the position of TS to the heliopause due to the slow solar wind in the inner heliosheath region. The dotted vertical line represents the rotation axis (magnetic pole) of the Sun. The arrows shows the direction of the HMF and the direction of rotation.

The basic structure of the HMF is that of an Archimedean spiral or otherwise called the Parker spiral. This spiral structure of the HMF is due to solar rotation. *Parker* (1958) derived an analytical expression to describe the HMF for $r \geq r_\odot$ and is given by

$$\mathbf{B} = B_o \left(\frac{r_o}{r}\right)^2 \left(\mathbf{e}_r - \frac{\Omega(r - r_\odot)\sin\theta}{V}\mathbf{e}_\phi\right), \tag{2.5}$$

where B_o is the HMF magnitude at Earth, r_o =1 AU, V the solar wind speed and $\Omega = 2.67 \times 10^{-6}$ rad.s^{-1}, the average angular rotation speed of the Sun. Also $\mathbf{e}_r$ and $\mathbf{e}_\phi$ are unit vector components in the radial and azimuthal directions respectively.

The above equation can be written in a more compact form in terms of the spiral angle ψ, the angle between the radial direction of the average HMF at a certain position. Where,

$$\tan\psi = \frac{\Omega(r - r_\odot)\sin\theta}{V}. \tag{2.6}$$

The ψ determines how tightly the HMF spiral would wound. A typical value of ψ is 45^o at Earth and tends to 90^o when $r \geq 10$ AU in the equatorial plane.

Substituting Equation 2.6 in Equation 2.5 gives,

$$\mathbf{B} = B_o \left(\frac{r_o}{r}\right)^2 (\mathbf{e}_r - \tan\psi \mathbf{e}_\phi)\,. \tag{2.7}$$

Spacecraft and Earth observations revealed the existence of a Parker spiral HMF at mid to low heliolatitudes, but the structure at polar regions is still under debate (see *Ness and Wilcox*, 1965; *Thomas and Smith*, 1980; *Roberts et al.*, 2007; *Smith*, 2011; *Sternal et al.*, 2011). A graphical representation of the Parker spiral is shown in Figure 2.15 for different polar angles 5^o (red), 45^o (green), 90^o (yellow), 135^o (blue) and 175^o (purple) with Sun at the centre. The magnetic field lines are seen compressed at some distance in the figure. This is due to a discontinuity called the termination shock (TS) which is discussed later. From the TS position onwards to the heliopause the HMF lines get compressed due to the slow solar wind in the inner heliosheath region.

The figure also shows that the magnetic field in the northern hemisphere of the Sun is directed outwards into interplanetary space and the magnetic field in the southern hemisphere is directed inward towards the Sun, which is called an $A > 0$ polarity cycle. An $A < 0$ polarity cycle is defined when magnetic field in the north is directed inwards towards the Sun and in the south away. The Sun switches its magnetic field polarity from $A > 0$ to $A < 0$ every ∼11 years forming a ∼22 year magnetic polarity cycle as discussed in Section 2.5.

From Equation 2.5 the magnitude of the HMF, B is given by,

$$B = B_o \left(\frac{r_o}{r}\right)^2 \sqrt{1 + \left(\frac{\Omega(r - r_\odot)\sin\theta}{V}\right)^2}, \tag{2.8}$$

or in compact form,

$$B = B_o \left(\frac{r_o}{r}\right)^2 \sqrt{1 + \tan^2\psi}. \tag{2.9}$$

The magnitude of the HMF also exhibits a ∼11 year cycle, correlated to the activity cycle of the Sun. Figure 2.16 shows a comparison of the ∼11 year cycle in B to the sunspot number for last 3 solar cycles. From the figure it follows that B (blue line) increases with an increase in sunspot number and decreases with a decrease in sunspot numbers forming a ∼11 year cycle. The magnitude of HMF at Earth is ∼5 nT during solar minimum conditions and the magnitude increases by a factor of ∼2 during solar maximum periods. The shaded area represents the period when there was not a well defined HMF polarity. The $A > 0$ and $A < 0$ shows the magnetic polarity during each solar cycle.

2.7.1 The modified Parker field

A Parker spiral is an oversimplified description for HMF at high heliolatitudes, since the radial field lines at the poles are in a state of unstable equilibrium. A small perturbation in this region can cause the field to collapse from a Parker spiral. Based on the state of the turbulent polar solar surface where the feet of the field lines appear, *Jokipii and Kota* (1989) presented a modified

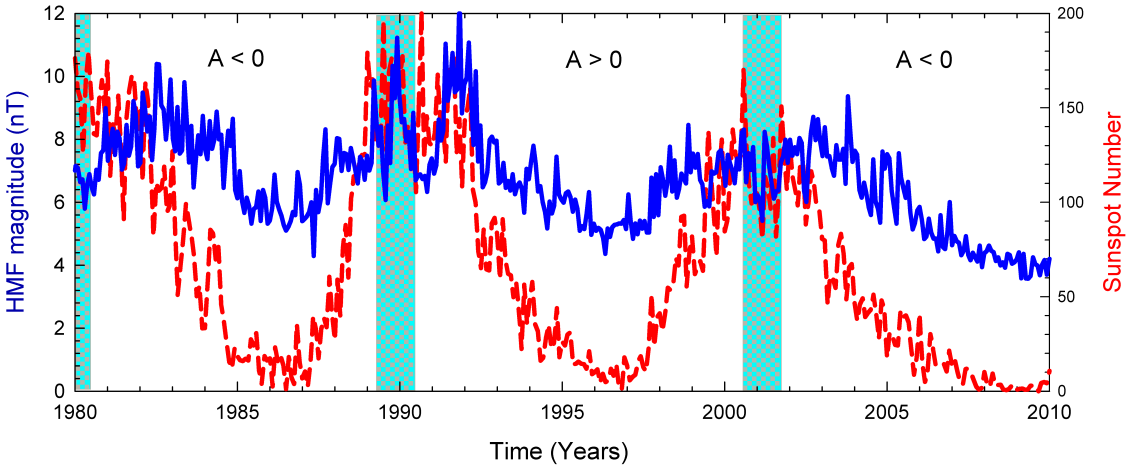

Figure 2.16: The observed 26 day averaged HMF magnitude (blue) at Earth compared to the observed monthly sunspot numbers (red). The shaded areas represent the periods where there were not a well defined HMF polarity. The HMF magnitude data is from: http://cohoweb.gsfc.nasa.gov and the sunspot number data is from: ftp://ftp.ngdc.noaa.gov.

Parker model. Since the turbulence on the solar surface cause foot points of the solar magnetic field to wander randomly, especially at polar regions, it creates a transverse component in the field. This component causes the field to vary from a pure Parker spiral to a highly irregular and compressed field. At the poles this results in a mean magnetic field magnitude greater than that of a pure Parker model. The modification of Parker model was proposed by *Jokipii and Kota* (1989) with an introduction of a parameter δ_m, which signifies the magnitude of the transverse magnetic field. The modified HMF expression can be written as,

$$B = B_o \left(\frac{r_o}{r}\right)^2 \sqrt{1 + \left(\frac{\Omega(r - r_\odot)\sin\theta}{V}\right)^2 + \left(\frac{r\delta_m}{r_\odot}\right)^2}. \tag{2.10}$$

For this study δ_m value is considered to be 0.001 (*Haasbroek and Potgieter*, 1995; *Hattingh*, 1998; *Ferreira*, 2002; *Langner*, 2004), for which the magnitude of the HMF changes substantially in the polar regions without altering the magnitude of the field in the equatorial regions. Ulysses measurements of the HMF in the polar regions qualitatively support this modification (*Balogh et al.*, 1995; *Heber and Potgieter*, 2008).

In this work, the diffusion coefficients are not directly expressed in terms of the modified magnetic field **B** but the drift coefficient is expressed in terms of this field, which is discussed in the next chapter. As a result of this modified magnetic field, the drift patterns which cosmic rays experience inside the heliosphere is altered by reducing the drift at the polar regions. This modified model is tested and applied by various authors, e.g. *Haasbroek et al.* (1995); *Ferreira* (2002); *Langner* (2004); *Ndiitwani* (2005); *Strauss* (2010); *Manuel et al.* (2011a,c)

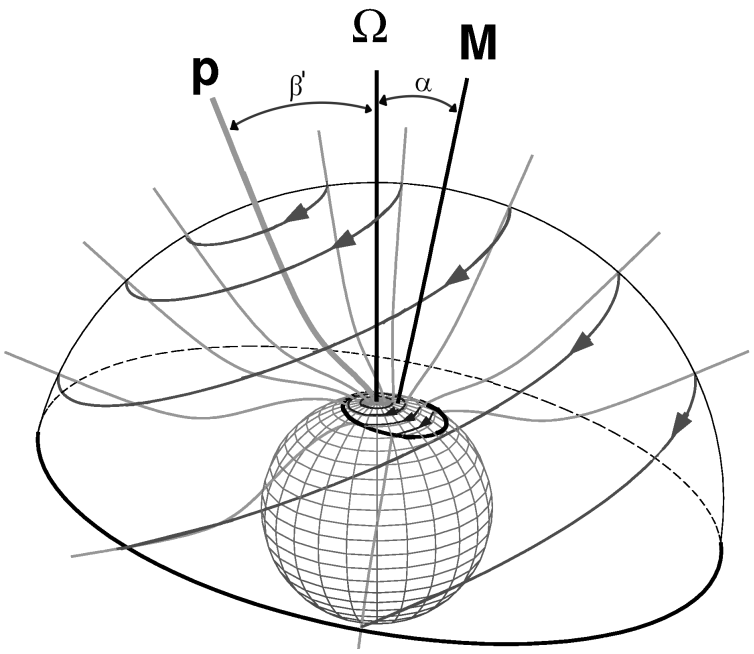

Figure 2.17: A schematic illustration of the expansion of magnetic field lines from a polar coronal hole in the Sun's northern hemisphere according to the model by *Fisk* (1996). The differential rotation of solar surface (inner sphere) magnetic flux elements is projected onto the solar wind source surface (outer sphere). From *Fisk et al.* (1999)

2.7.2 The Fisk-type heliospheric magnetic field

As discussed in Section 2.2 the Sun does not rotate like a rigid body, like Earth, but has a differential rotation. The Sun rotates faster at the equator and slower towards the poles (*Bartusiak*, 1994). Due to this differential rotation of the Sun, the foot points of the HMF on the solar surface also under go differential rotation. Considering this phenomenon, *Fisk* (1996) proposed a different model of HMF, later on called the Fisk HMF or Fisk field. In this model, the field lines will move through a coronal hole due to the differential rotation and experience a subsequent non-radial expansion from the solar surface. This in turn results in large excursions in latitude and longitude of field foot-points on the solar wind source surface, where the solar wind flows radially outward into the heliosphere. These excursions in foot-point position, particularly in heliographic latitude, can provide direct magnetic connection between the high and low heliolatitudes i.e. the magnetic field lines at high latitudes can be connected directly to corotating interactions regions (CIRs) in the solar wind at lower latitudes.

The basic geometry of the Fisk field in the northern hemisphere is shown in Figure 2.17. The magnetic field configuration is centred on the **M** axis which is offset from the rotation axis $\mathbf{\Omega}$ by an angle α, called the tilt angle. A field which originates from the heliographic pole will experience non radial expansion and it will be bent back and penetrate the source surface as the field line **p**, which is misaligned to the rotation axis $\mathbf{\Omega}$ by an angle β'. All other field lines differentially rotate in a clockwise direction about the polar field line **p** with a differential

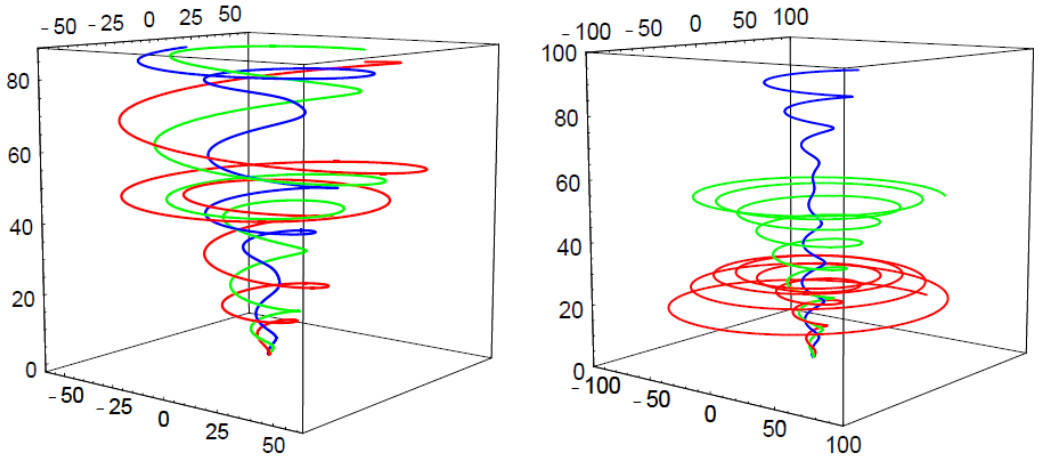

Figure 2.18: A graphical illustration of the HMF lines of the type I Fisk field (left panel) and type II Fisk field (right panel). The field lines in both panels originate at a north heliolatitude of 60^o and at different longitudes. In both case the solar wind speed is 800 km.s^{-1} and the dimension of the cubes are in the unit, AU. From *Burger and Hattingh* (2001)

rotation rate ω and expand non-radially into the rigidly rotating source surface, which rotates at a rate Ω. Hence the foot-points on the source surface happen to be rotating about $\mathbf{p}$ and $\mathbf{\Omega}$, since $\mathbf{p}$ rotates rigidly about $\mathbf{\Omega}$ (see e.g. *Zurbuchen et al.*, 1997; *Fisk et al.*, 1999; *Burger*, 2005; *Zurbuchen*, 2007; *Burger et al.*, 2008; *Engelbrecht*, 2008; *Sternal et al.*, 2011).

The three components of the Fisk field are given by (*Zurbuchen et al.*, 1997),

$$\begin{aligned} B_r &= B_o \left(\frac{r_o}{r}\right)^2, \\ B_\theta &= B_r \frac{(r - r_{ss})\omega}{V} \sin\beta' \sin\left(\phi + \frac{\Omega(r - r_{ss})}{V}\right), \\ B_\phi &= B_r \frac{(r - r_{ss})}{V}\left(\omega \sin\beta' \cos\theta \cos\left(\phi + \frac{\Omega(r - r_{ss})}{V}\right) + \sin\theta(\omega\cos\beta' - \Omega)\right), \end{aligned} \tag{2.11}$$

where r_{ss} is the radius of the solar source surface.

Burger and Hattingh (2001) classified the Fisk field into two types namely, Fisk type I field and Fisk type II field. The field is called a type I field when the HMF is described by Equation 2.11 and type II field when it is described by the same equation but with a β value of 90^o. A graphical representation of the type I and II fields are shown in Figure 2.18, where both the HMF field lines originate at a north heliolatitude of 60^o but from different longitudes. A solar wind speed of 800 km.s^{-1} is assumed and the dimension of the cubes are in AU.

Later *Burger and Hitge* (2004) presented a new model of HMF by combining the Parker HMF and Fisk HMF, called a Fisk-Parker hybrid field. These authors modelled the HMF such a way that its structure becomes a pure Fisk field in the mid heliolatitudes and becomes a pure Parker HMF in the equatorial plane and at the poles. However, the regions between mid heliolatitude and equatorial plane, and mid heliolatitude and poles are a combination of the Fisk and Parker model (*Burger and Hattingh*, 2001; *Burger*, 2005; *Burger et al.*, 2008; *Engelbrecht*, 2008; *Hitge and*

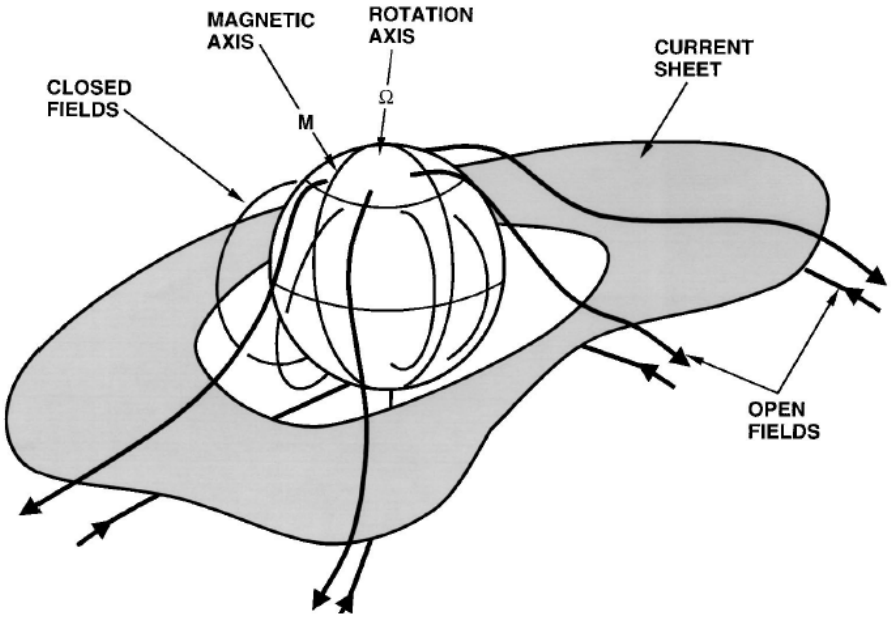

Figure 2.19: A schematic representation of the HCS, as shaded area. The HCS separates the open fields from the north and south solar magnetic poles. Open field lines has only one end on the solar surface but the closed field lines has both the ends on the solar surface. Also the magnetic and rotation axis of the Sun is shown. From *Smith* (2001).

Burger, 2010).

A HMF with a meridional component (Fisk field) leads to a more complicated form of the transport equation than when a Parker-type field is used. A Fisk field is inherently three-dimensional and time-dependent which results in an increase in the number of mixed derivatives, which in turn results easily in an unstable numerical code used to solve the transport equation (e.g. *Kota and Jokipii*, 1997, 1999; *Burger and Hattingh*, 2001). Due to the complexity of this field, it is not incorporated in the numerical modulation model that is used in this work. The Fisk HMF is a well debated topic due to the uncertainty of its existence based on the observations (*Roberts et al.*, 2007). However, recently *Sternal et al.* (2011) presented a study which supports a possible existence of Fisk field, based on Ulysses/KET electron observations.

2.8 The heliospheric current sheet

The heliospheric current sheet (HCS) is a boundary structure (narrow layer) encircling the Sun. It separates the oppositely directed open magnetic field lines that originate from the solar surface. These open magnetic field lines have only one end attached to the Sun and it stretches towards the interplanetary space, while a closed field line has both its ends attached to the Sun. Since Sun is a magnetic dipole, the magnetic field lines in one hemisphere has a polarity exactly opposite to that found in the other hemisphere. The HCS is a unique structure and it represents the magnetic equator of the heliosphere which divide the heliosphere into two

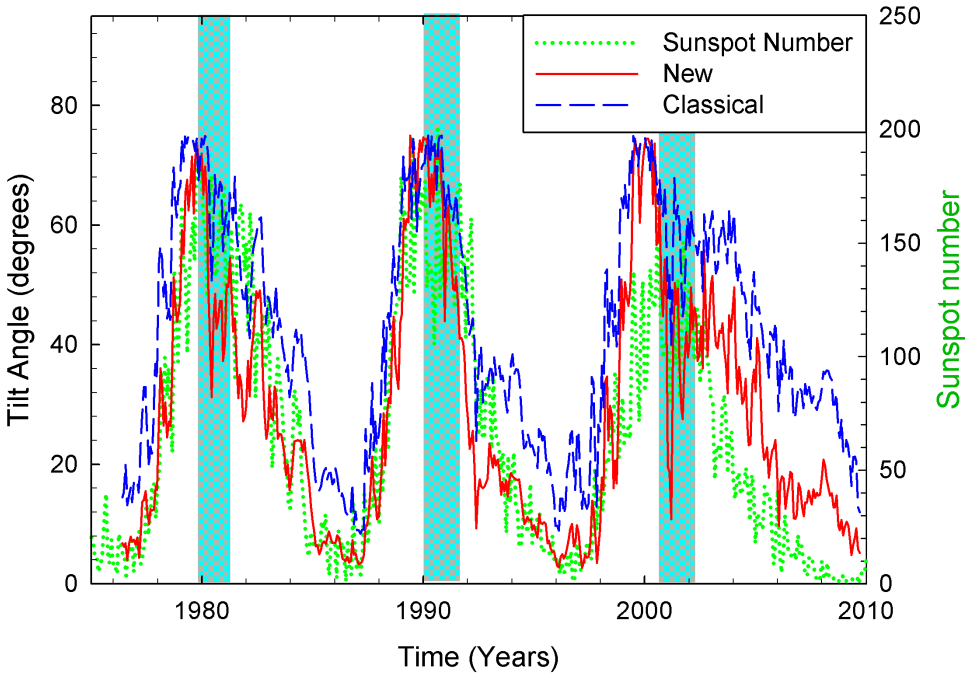

Figure 2.20: The two different model tilt angle α, namely "classical" (blue dashed line) and "new" (red solid line) are shown as a function of time from 1977 until 2010. Both the tilt angles are compared to the yearly sunspot number (green dotted line). A ∼11 year cycle correlated to the sunspot cycle can be seen. Tilt angle data from: http://wso.stanford.edu and yearly sunspot data from:ftp://ftp.ngdc.noaa.gov.

magnetic halves. At 1 AU the thickness of the HCS is ∼10000 km, it is so thin and therefore often assumed to be of zero thickness. The width of the HCS increases nearly proportional with distance from the Sun (see e.g. *Balogh and Smith*, 2001; *Smith*, 2001; *Czechowski et al.*, 2010).

Figure 2.19 shows the HCS as a shaded area which separates the open magnetic fields originating from north and south solar magnetic poles. The closed field lines are located at low and mid heliolatitudes and lie inside the HCS structure. Also the magnetic axis and the rotation axis of the Sun are shown, which are tilted by an angle called the HCS tilt angle α.

As the Sun rotates, it forms a current sheet which oscillates about the heliographic equator to form a series of peaks and valleys which spiral outwards. The shape of the HCS is a combined effect of the tilt angle, solar rotation and solar wind speed. The waviness of the HCS is thus correlated to the solar activity. During solar maximum periods, the tilt angle increases to $\sim 75^o$ and which in turn increase the waviness (height of the waves) of the HCS. For a low solar activity period the tilt angle decreases to $\sim 5^o$ thereby decreasing the waviness of the HCS. Concerning cosmic ray transport inside the heliosphere, the tilt angle is an important factor which affect cosmic ray propagation. Figure 2.20 shows the time-dependence in tilt angle using two different models of tilt (*Hoeksema*, 1992), the "classical" and "new (radial)". To compute the tilt angle, the classical model used line-of-sight boundary conditions with a source surface

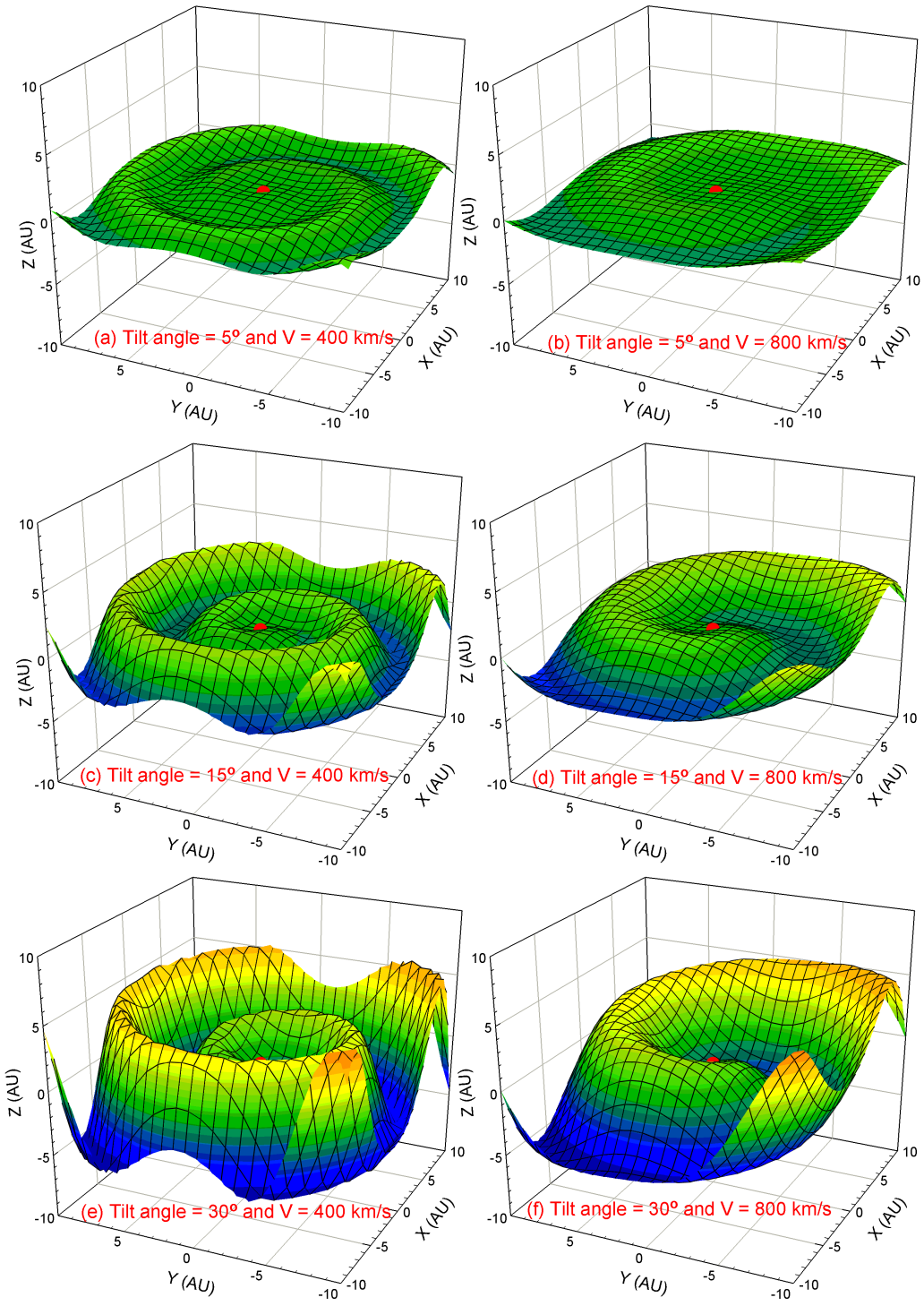

Figure 2.21: An idealised graphical illustration of the 3D structure of HCS for three different tilt angle (α) values when a slow and fast solar wind speed (V) persist inside the heliosphere. Shown here is a cubical cut of the heliosphere with the Sun at the centre (red dot) and each side equal to 20 AU. Each image from (a)-(f) shows the structure of the HCS for $\alpha = 5^o, 15^o$ and 30^o when both $V = 400$ km.s^{-1} (left panels) and $V = 800$ km.s^{-1} (right panels) solar wind speed persist. The spirals of the HCS stretches with an increase in V. So a less tightly wound structure is seen for $V = 800$ km.s^{-1} when compared to $V = 400$ km.s^{-1}.

at $2.5r_\odot$ while the new model used the radial boundary conditions at the photosphere and with a source surface at $3.5r_\odot$. From the figure it follows that the tilt angle varies from $\sim 5^o - 10^o$ during solar minimum periods to $\sim 75^o$ during solar maximum periods, correlated to the ~11 year sunspot cycle.

The radially out-flowing solar wind also effects the HCS structure in such a way that an increase in solar wind speed stretches the HCS spirals further away since the HCS is carried together with the HMF by the solar wind. The structure of the HCS for different tilt angles and solar wind speeds are shown in Figure 2.21 with the Sun as a red dot at the centre of a cube with sides of dimension 20AU. The HCS does not stop at the given distance but continues out into the heliosphere. Different scenarios corresponding to different tilt angle values of 5^o, 15^o and 30^o respectively are compared, assuming a slow wind speed of 400 km.s^{-1} (left panels) and a fast wind speed of 800 km.s^{-1} (right panels). From the figure it follows that with an increase in tilt angle from 5^o to 30^o the waviness (height of the wave) of the HCS increases for both slow and fast solar wind. Also it can be see that with an increase in solar wind speed from 400 km.s^{-1} to 800 km.s^{-1} the wavy spirals stretches away further (distance between two peaks or valleys is increased). So a less tightly wound HCS structure is seen for a fast solar wind (see e.g. *Balogh and Smith*, 2001; *Riley et al.*, 2002; *Czechowski et al.*, 2010).

The position and inclination of the HCS can be inferred from the magnetic neutral line in the source surface (*Smith*, 2001). Figure 2.22 shows contour plots of the coronal magnetic field, computed using Potential Field Source Surface (PFSS) model (*Schatten et al.*, 1969), on the source surface located at $2.5r_\odot$. These contour plots are for October 2009 (Carrington rotation 2089) and February 2011 (Carrington rotation 2107) which correspond to a low solar activity (lower panel) and high solar activity (upper panel) periods. The HCS can be identified on each panel as the black line separating regions of opposite polarity, shown as shades of grey colour. The magnetic equator which corresponds to the neutral line (thick black line) is seen staying close to the solar equator during the low solar activity period. However, during solar maximum period this neutral line can be seen as reaching higher heliolatitudes. The inclination of the HCS can be found by calculating the difference between the maximum latitudes reached by this neutral line.

Magnetic field observations on both Voyager spacecraft revealed the continuous presence of the HCS from the inner to outer heliosphere (*Burlaga and Ness*, 1998). Ulysses observations confirmed that during the maximum solar activity period the HCS extends to high heliolatitudes (*Balogh and Smith*, 2001; *Smith*, 2001). During periods of high solar activity the magnetic dipole like appearance of the Sun changes to even a quadrupole nature which results in a possibility of forming multiple HCS (*Kota and Jokipii*, 2001a; *Crooker et al.*, 2004; *Foullon et al.*, 2009). The HCS rotates along with the Sun once every ~27 days and extends throughout the heliosphere (see *Smith*, 2001; *Zurbuchen*, 2007; *Balogh and Erdos*, 2011, for a review).

The HCS has a significant effect on the cosmic ray transport in the heliosphere. It effect the drift motions of the cosmic rays. The significance of cosmic ray drifts was pointed out by

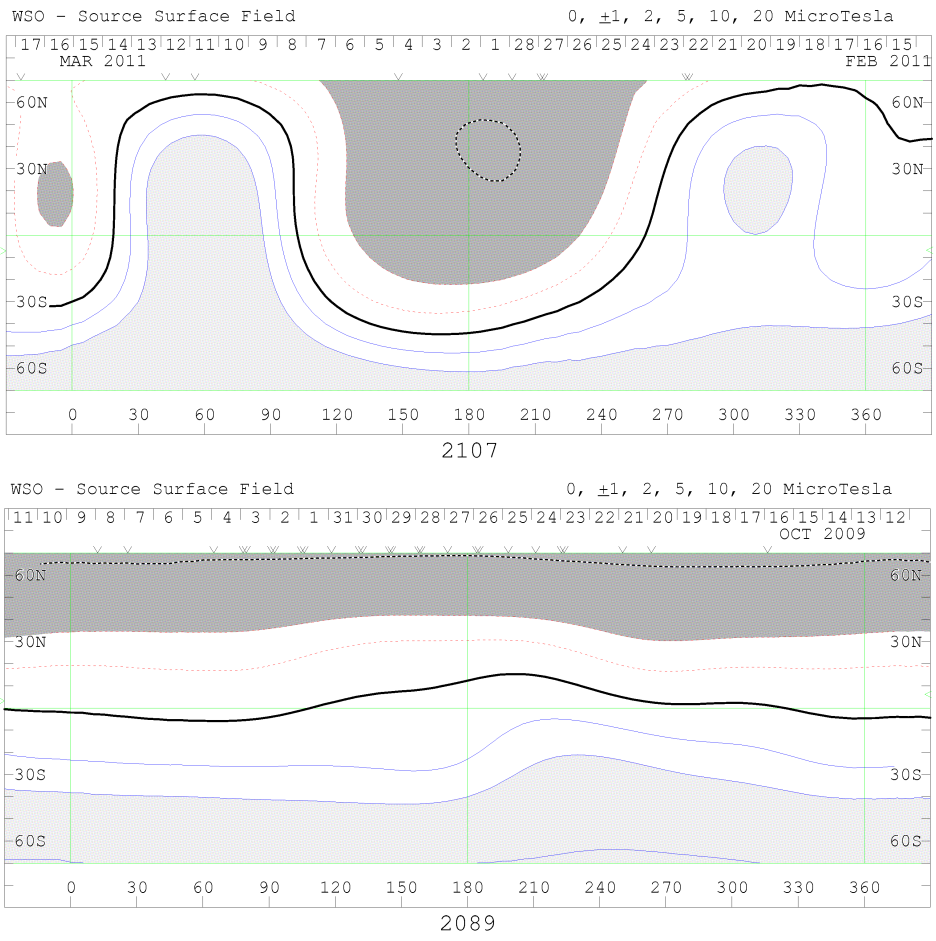

Figure 2.22: Contour plots of the coronal magnetic field computed using Potential Field Source Surface (PFSS) model (*Schatten et al.*, 1969) on a source surface at $2.5r_{\odot}$. These contour plots are for October 2009 solar minimum (lower panel) and for an increased solar activity on February 2011 (upper panel). The thick black line on both panels corresponds to the neutral line. The magnetic polarities of each solar hemispheres are represented by light grey (magnetic field directed inwards to the Sun) and dark grey (magnetic field directed away from the Sun) colours. Below and above the neutral lines opposite polarities are seen, in this case corresponding to an $A < 0$ HMF polarity cycle. Images from http://wso.stanford.edu.

Jokipii et al. (1977), *Potgieter* (1984) and *Potgieter and Moraal* (1985). Due to the gradients of the magnetic field around the HCS and the reversal of the direction of the magnetic field from one side of the HCS to the other, cosmic rays experience an effective drift along the HCS. The direction of the particle drift depends on the polarity of the solar magnetic field which changes every ∼11 years. For an $A > 0$ polarity cycle, positively charged particles drift outwards along the HCS and negatively charged particles drift in along the HCS, and the opposite is observed during an $A < 0$ polarity cycle. A detailed discussion on this is given in Chapter 3.

Cosmic ray transport inside the heliosphere was numerically simulated with a modulation model including a realistic 3D HCS by several authors like *Kota and Jokipii* (1983); *Hattingh and Burger* (1995a); *Pei et al.* (2012); *Strauss et al.* (2012a). For a constant and radial solar wind speed

Jokipii and Thomas (1981) derived an equation for the HCS given as,

$$\theta' = \frac{\pi}{2} + \sin^{-1}\left(\sin\alpha \sin\left[\phi + \frac{\Omega(r - r_o)}{V}\right]\right), \tag{2.12}$$

where θ' is the polar angle of the HCS and ψ the azimuthal angle. For a smaller tilt angle the above equation reduces to,

$$\theta' \cong \frac{\pi}{2} + \alpha \sin\left[\phi + \frac{\Omega(r - r_o)}{V}\right]. \tag{2.13}$$

The global effects of HCS on cosmic ray transport has been simulated by several authors, using 2D numerical modulation models (*Potgieter*, 1984; *Burger*, 1987; *Hattingh*, 1998; *Ferreira*, 2002; *Langner*, 2004; *Strauss*, 2010). In Chapter 3, the 2D simulation of the HCS used for this study is discussed.

The polarity of the HMF is included in Equation 2.7 by modifying it into,

$$\mathbf{B} = AB_o\left(\frac{r_o}{r}\right)^2 (\mathbf{e}_r - \tan\psi\mathbf{e}_\phi)\,[1 - 2H(\theta - \theta')]. \tag{2.14}$$

Here, $A = \pm 1$, is a constant determining the polarity of the HMF and which changes every 11 years. The period when the HMF in the northern solar hemisphere is pointed outwards and towards the Sun in the southern hemisphere called the $A > 0$ polarity cycle, A has the value $+1$. For an $A < 0$ polarity cycle, that is the period when HMF in the solar northern hemisphere is pointed inwards to the Sun and outwards in the south hemisphere, A has the value -1. The $H(\theta - \theta')$ is the Heaviside step function and is given by,

$$H(\theta - \theta') = \begin{cases} 0 & \text{when } \theta < \theta' \\ 1 & \text{when } \theta > \theta'. \end{cases} \tag{2.15}$$

This function changes the HMF polarity across the HCS. Numerical instability occurs when this function is directly used, so an approximation of this function as proposed by *Hattingh* (1998) is used in this study and is given by,

$$H'(\theta) \approx \tanh\left[2.75(\theta - \theta')\right]. \tag{2.16}$$

2.9 The boundaries of the heliosphere

Helios is the ancient Greek word for the Sun and the heliosphere is the entire region of space influenced by the Sun and its magnetic field called the HMF. The radially expanding hot upper atmosphere of the Sun, the solar wind, carries out along with it the HMF into the interplanetary space and towards the local interstellar medium (LISM). The HMF is responsible for the modulation of cosmic rays in the heliosphere. When the solar wind encounters the LISM, it creates a tear drop shaped bubble or cavity with the Sun and its planets, comets, asteroids, etc inside this cavity, called the heliosphere. The tear drop shape of the heliosphere is due to

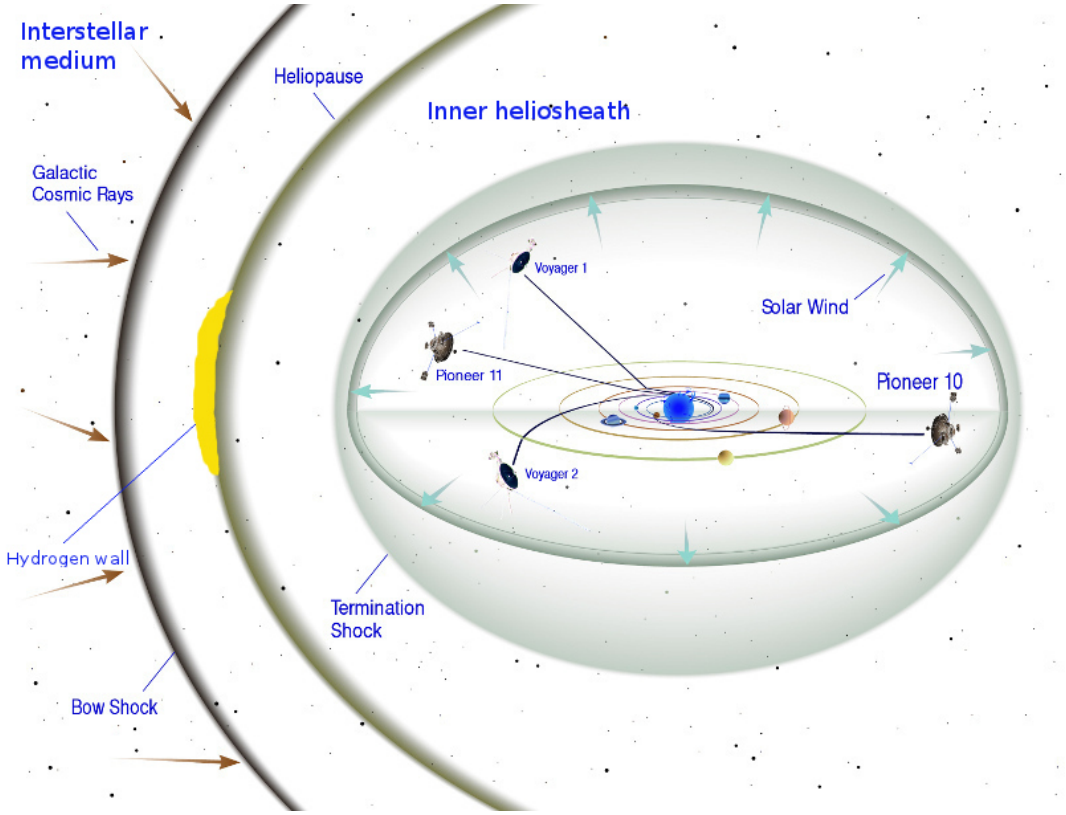

Figure 2.23: A graphical representation of the heliosphere. From http:www.nasa.gov.

the interstellar wind which deflects around it. A graphical representation of the heliosphere is shown in Figure 2.23.

The location where the solar wind pressure is balanced by the LISM pressure is called heliopause. The heliosphere is not a symmetric structure, it varies in shape depending on various parameters like the solar activity, interstellar wind and solar wind etc. The best indication of the boundaries of the heliosphere at the present time was obtained when NASA's Voyager 1 and Voyager 2 spacecraft crossed the TS, one of its key outer boundaries, in December 2004 and August 2007. The distance of Voyager 1 from the Sun was then at ∼94 AU and Voyager 2 was at ∼84 AU (*Decker et al.*, 2005; *Richardson et al.*, 2008; *Stone et al.*, 2008). Figure 2.23 shows the features like solar wind and different boundaries of the heliosphere. Also the trajectories of outer heliosphere exploring Voyagers spacecraft are shown. Apart from the Voyager observations of a TS asymmetry, recent theoretical work done by *Opher et al.* (2009b) and *Pogorelov et al.* (2009b) suggests a possible asymmetry in the two hemispheres due to an external pressure resulting from the interstellar magnetic field. A detailed discussion on heliospheric asymmetry is given in Chapter 8.

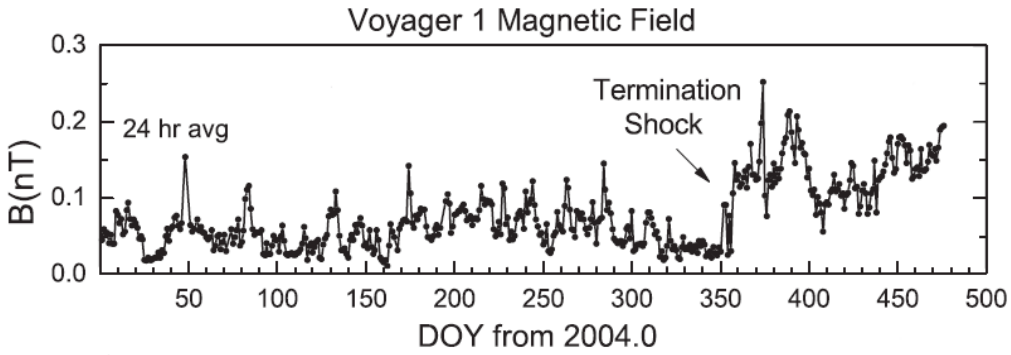

Figure 2.24: Daily averaged magnetic field strength B as measured by the Voyager 1 spacecraft as a function of time. The TS position is shown by an arrow where a sudden increase in B was observed. Time is shown in days from the beginning of 2004 and DOY means day of year. From *Burlaga et al.* (2005).

2.9.1 The termination shock

The Sun is moving through the LISM with a speed of ∼25.5 km.s^{-1} according to *Lallement et al.* (2005) and ∼23.2 km.s^{-1} according to *McComas et al.* (2012). As it moves, its radial out-flow of solar material, the highly supersonic solar wind encounters the near-stationary LISM. Due to this encounter, the cool supersonic solar wind slows down to a hotter subsonic solar wind and is then diverted downstream to form a heliotail. The shock wave that is formed from this encounter is called the termination shock (TS) and is the location where the solar wind becomes subsonic. The TS forms a shell like region inside the heliosphere where the solar wind speed inside this shell is supersonic and outside subsonic (see Figure 2.23). The TS causes a discontinuity in different solar wind parameters, e.g. a sudden solar wind speed decrease, a sudden increase in density and an increase in temperature. The HMF is also compressed and a discontinuity in magnetic field magnitude is also measured (*Muller et al.*, 2006; *Richardson et al.*, 2008).

The TS has been crossed by both Voyager 1 and Voyager 2 spacecraft (e.g. *Stone et al.*, 2005, 2008). The observations from these spacecraft revealed the position of TS during the time of spacecraft passage. Also the asymmetry in the shape of TS and the heliosphere as a whole is observed and modelled. Prior to both TS crossing, the Voyagers observed streaming of energetic particles in a region named foreshock. The foreshock is described as a region upstream of the TS populated by energetic particles that originate mainly from the TS and beyond, which exhibit large and frequent intensity fluctuations (*Decker et al.*, 2005). Voyager 1 entered the foreshock region at a heliographic latitude 34^{o}N and at a helioradius 85 AU. While Voyager 2 entered the foreshock region at heliographic latitude 26^{o}S and at a helioradius 75 AU. Later, Voyager 1 crossed the TS at a helioradius of 94 AU on 16 December 2004 (*Burlaga et al.*, 2005; *Decker et al.*, 2005; *Stone et al.*, 2005) and Voyager 2 crossed the TS at a helioradius of 84 AU between 30 August and 1 September 2007, 10 AU closer to the Sun than Voyager 1 (*Burlaga et al.*, 2008; *Richardson et al.*, 2008; *Stone et al.*, 2008).

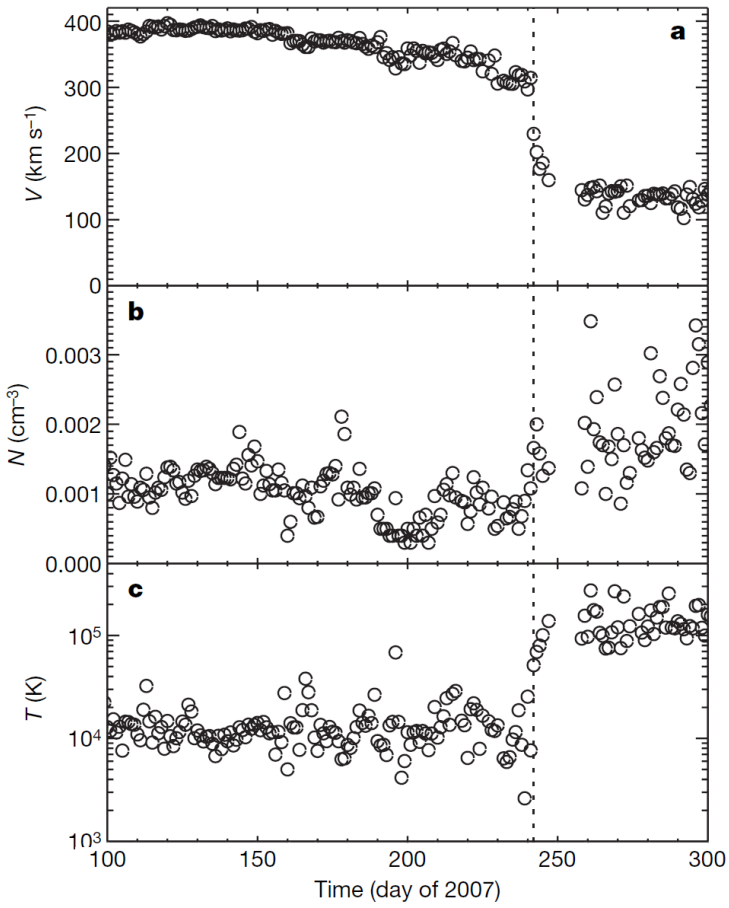

Figure 2.25: Daily averaged (a) radial solar wind speed V, (b) density N and (c) temperature T as measured by plasma experiment on-board Voyager 2 spacecraft is shown as a function of time. The TS position is shown as a dashed vertical line. A sudden increase or decrease in these measured parameters are seen at the TS position. From *Richardson et al.* (2008).

The discontinuity in heliospheric parameters measured by both the Voyagers while crossing the TS are shown in Figure 2.24 and 2.25. The working magnetic field instrument on-board Voyager 1 measured the magnetic field strength B during the TS crossing and is shown in Figure 2.24 in terms of days of the year (DOY), from day 1 of 2004 to day 110 of 2005. From the figure it follows that the daily averaged B increases suddenly at around day 350 when Voyager 1 encounters the TS. A compression ratio s_k of 3.05 across the TS is found by *Burlaga et al.* (2005) but due to uncertainty associated with the choice of averaging interval and other systematic errors, a s_k in the range from 2 to 4 is plausible. The compression ratio $s_k = \frac{B_2}{B_1}$, where B_1 is the magnetic field strength before crossing the TS and B_2 is the magnetic field strength after crossing the TS.

Figure 2.25 shows the measurements from the plasma experiment instrument on-board Voyager 2 during the TS crossing. The figure shows daily averaged (a) radial solar wind speed V (top panel), (b) density N (middle panel) and (c) temperature T (bottom panel) measured by Voyager 2 spacecraft as a function of time. The TS position is shown as a dashed vertical

line. A sudden increase or decrease in these measured parameters are seen at the TS position. The solar wind speed decreases from ∼400 km.s^{-1} to ∼300 km.s^{-1}, the density is increased by a factor of two and the temperature is increased to ∼100000 K. The compression ratio s_k in the range from 1.6 to 2.4 is calculated during the Voyager 2 TS crossing (*Richardson et al.*, 2008). Note that the plasma experiment on-board Voyager 1 is not functional, so solar wind parameters are not available for that spacecraft.

A TS position of 10 AU closer to the Sun along the Voyager 2 trajectory, compared to the Voyager 1, showed a possible asymmetric structure of the shock and/or a time-dependence in shock position. The first could be due to an interstellar magnetic field that is tilted by 60^o from the flow direction of the LISM. This results in a heliosphere where the southern portion of the heliosphere are being pushed inwards by magnetic pressure compared to the northern portion. Another possible reason for the difference in measured shock position could be the solar cycle where the shock oscillate with time, depending on solar activity (*Scherer et al.*, 2006b; *Snyman*, 2007; *Richardson et al.*, 2008; *Webber and Intriligator*, 2011). However, the observed ∼10 AU difference between the position of the TS along the Voyager 1 and 2 trajectory possibly suggests both time-dependent oscillations of the TS and an asymmetry due to external pressures resulting from the interstellar magnetic field (*Opher et al.*, 2009b; *Pogorelov et al.*, 2009b). Also an encounter with global merged interaction regions may cause the TS position to oscillate as much as ∼3 AU in the upwind direction (*Potgieter*, 2008). A detail discussion on asymmetry in TS and the heliosphere is given in Chapter 8.

In this work, a spherically symmetric TS at a stationary position is assumed first and later a time-dependent TS position is implemented (*Langner and Potgieter*, 2005; *Lange et al.*, 2006; *Ngobeni and Potgieter*, 2011). The time-dependence in TS is discussed later in Chapter 10. Also a compression ratio as suggested by *Burlaga et al.* (2005) and *Richardson et al.* (2008) is used in this work. Note that the re-acceleration of galactic cosmic rays at the TS is not considered.

2.9.2 The heliopause and the bow shock

The second heliospheric boundary after the TS (from the Sun outward) is the heliopause. In space, plasma of different origin does not easily mix because of the magnetic fields associated with it (*Balogh et al.*, 2008). Due to this reason when the solar wind encounters the interstellar medium, a boundary layer is formed and this boundary layer is called the heliopause, which separates the solar from the local interstellar plasma. At the heliopause, the pressure of the outflowing solar wind balances the interstellar medium pressure leading to equal pressure on both sides and therefore plasma is not transported across. It could be considered as the outer boundary of the heliosphere (*Potgieter*, 2008).

This outer shell of the heliosphere is shown in Figure 2.23. At the heliopause the Sun's influence (solar wind and HMF) ends. The solar wind encounters with the interstellar wind causes the solar wind to slow down, turn and then to flow down the tail of the heliosphere. This solar

wind, which are turned and flowing towards the heliotail, eventually flow parallel compared to the interstellar wind. According to *Krimigis et al.* (2011), Voyager 1 is currently experiencing a zero radial solar wind speed from April 2010 at a heliocentric distance of 113.5 AU. From this it follows that the spacecraft is near the heliopause and these authors suggest that the heliopause position is expected to be around ∼121 AU. See e.g. *Richardson and Burlaga* (2011) for a review.

Beyond the heliopause, depending on the pressure of the surrounding LISM, a bow shock could form where the interstellar plasma is decelerated from supersonic to subsonic speed (*Ferreira et al.*, 2007b). It is a shock region outside the heliosphere, see Figure 2.23. See *Balogh et al.* (2008); *Zank et al.* (2009); *Richardson and Burlaga* (2011) for a review. A bow shock is absent if a subsonic interstellar wind flows (*Liewer et al.*, 1996; *Zank et al.*, 1996b) and it exists only for a supersonic interstellar wind with an interstellar magnetic field strength less than 3 μG (*Pogorelov et al.*, 2008b). However, a supersonic interstellar flow with interstellar magnetic field strength greater than 3 μG prevents the formation of the bow shock (*Heerikhuisen and Pogorelov*, 2011). If such a shock exists, the typically assumed location of the bow shock is ∼300 to ∼400 AU, in the heliocentric nose direction (*Scherer and Fahr*, 2003b). However, recent observations from the Interstellar Boundary Explorer (IBEX) spacecraft suggest that because of the slower relative motion (∼23.2 km.s^{-1}) of the Sun with respect to the interstellar medium, it produces less dynamic pressure and may result in no bow shock but rather a bow wave (*McComas et al.*, 2012). See *Balogh et al.* (2008); *Zank et al.* (2009); *Richardson and Burlaga* (2011) for reviews.

2.9.3 The heliosheath

The region between the TS and the bow shock/wave with subsonic plasma speed and high density (compared to region inside the TS) is called the heliosheath. The heliosheath can be divided into two parts, namely the inner and outer heliosheath. The inner heliosheath is the volume of space between the TS and the heliopause and is a turbulent region where matter piles up as the solar wind presses outward against the interstellar matter, see Figure 2.23. The outer heliosheath is the volume of space between the heliopause and the bow shock/wave (*Scherer et al.*, 2011).

The temperature in the inner heliosheath ranges from 50000-150000 K and the solar wind speed fluctuates from 100 to over 250 km.s^{-1} with an average value of about 150 km.s^{-1}. According to Voyager 2 observations, these fluctuations in solar wind speed decreased with distance (*Richardson and Burlaga*, 2011). The most peculiar feature of the heliosheath is the large increase in the variability of B in this region (*Burlaga et al.*, 2006, 2007). Both Voyager 1 and Voyager 2 observed a large change in the magnitude of B on a scale of several hours or less (*Burlaga and Ness*, 2011).

Interstellar protons just outside the heliopause are heated and compressed by strong plasma interactions. There is also interstellar neutrals flowing in and gets ionised by charge exchange.

The reactions between the protons and the interstellar neutrals transmit high temperatures and high densities to the neutrals thus creating a region called a hydrogen wall. The hydrogen wall is seen between the heliopause and the bow shock/wave, see Figure 2.23. The hydrogen wall is a structure in the outer heliosphere that can be detected and studied observationally (see *Wood et al.*, 2004; *Muller et al.*, 2006; *Balogh et al.*, 2008; *Zank et al.*, 2009).

The heliosheath largely modulates cosmic rays entering the heliosphere (see e.g. *Langner et al.*, 2003, 2004, 2006). Both the Voyagers are at present exploring this region (see *Scherer and Fahr*, 2003b; *Baranov*, 2009; *Richardson and Burlaga*, 2011). The effect of this turbulent region (as well as the supersonic solar wind region) on cosmic ray intensities is the topic of this work.

2.10 Cosmic rays

Cosmic rays are energetic charged particles in the heliosphere. Cosmic ray research began when Victor Hess, on 12 August 1912, measured the ionising radiation in the atmosphere with an electroscope in a hydrogen filled balloon. This balloon went up to an altitude of 5.35 km and Hess observed that at ∼5.0 km the measured rate was more than twice the value on Earth's surface. From this observations Hess concluded that this radiation, which we now call cosmic rays, are coming from outside the Earth's atmosphere.

Cosmic rays are detected at Earth using neutron monitors. When cosmic rays enter Earth's atmosphere, the primary cosmic rays collide with the atmospheric molecules and produce showers of secondary particles. Neutron monitors detect these secondary particles and give an indication of the primary cosmic ray flux (*Moraal et al.*, 2000; *Moraal and Stoker*, 2010).

Within the heliosphere, cosmic rays of different origin is identified. So these charged particles can be classified into four main populations, namely,

1. Galactic cosmic rays (GCRs): This population of energetic particles comes from outside the heliosphere evenly from all directions. They are accelerated by shock waves in the galaxy (like the supernova remnants, pulsars, active galactic nuclei) to very high energies and travel at nearly the speed of light (*Axford*, 1981; *Bell*, 1978a,b; *Busching and Potgieter*, 2008; *Fisk and Gloeckler*, 2012). When they arrive at Earth these particles consist of ∼98% fully ionised nuclei, primarily protons, and ∼2% electrons, positrons and a few anti-protons. GCRs are considered as those particles with energies up to 10^{15} eV, above this they are considered as extragalactic cosmic rays which originates from extra galactic sources (see *Schlaepfer*, 2003; *Aharonian et al.*, 2012). The research topic of this work is the modulation of the GCRs inside the heliosphere (see e.g. *Potgieter*, 2010; *Strauss et al.*, 2012b, for a review). Note that only energies/nucleon below 10^9 eV are considered for this study.

2. Solar energetic particles (SEPs): These particles are of solar origin. They are accelerated mainly by solar flares, coronal mass ejections and shocks in the interplanetary medium.

They are observed only occasionally at Earth (usually only for several hours) mainly during maximum solar activity periods. The CMEs which expand outward from the Sun are capable to drive interplanetary shock waves that can re-accelerate SEPs to form large gradual SEP events. The SEP events are observed rarely reaching high energies of ∼1 GeV for protons and ∼100MeV for electrons (see e.g. *Forbush*, 1946; *Balogh et al.*, 2008; *Cliver*, 2008; *Grechnev et al.*, 2008; *Usoskin*, 2008). SEPs are not considered for this study.

3. Anomalous cosmic rays (ACRs): ACRs are those cosmic ray particles which were initially neutral interstellar gas flowing into the heliosphere. The neutral particles from the LISM flow into the heliosphere without getting deflected by the HMF. These neutral particles get ionised relatively close to the Sun by photo-ionisation or by charge exchange and then these ions (called pick-up ions) are transported to the outer heliosphere. These charged particles then gets accelerated up to ∼100 MeV at the solar wind TS to become ACRs (*Fisk et al.*, 1974; *Cummings et al.*, 2002). The low energy ACRs are mostly singly ionised particles but the presence of multiply charged ACRs are also reported (*Mewaldt et al.*, 1996; *Strauss*, 2010). The elements like hydrogen and helium which are abundant in the neutral interstellar gas are also the most abundant species of ACR component observed (see e.g. *Fichtner*, 2001; *Florinski*, 2009; *Gloeckler et al.*, 2009; *Potgieter*, 2010; *Strauss et al.*, 2010b, for a review). ACRs are also not considered for this work.

4. Jovian electrons: They are energetic electrons which are continuously emitted into the interplanetary space by Jupiter's magnetosphere. This population of energetic particles were detected during the approach of the Pioneer 10 spacecraft towards Jupiter. This spacecraft went as close as 1 AU of Jupiter. The observations found that the Jovian magnetosphere, at ∼5 AU in the ecliptic plane, is a strong source of electrons with energies up to ∼30 MeV and propagate along and across the HMF. They are observed at Earth and up to ∼10 AU. More recently, the Ulysses spacecraft confirmed that Jupiter is a strong source of 30 MeV electrons.(see e.g. *Ferreira et al.*, 2001; *Ferreira*, 2005; *Heber and Potgieter*, 2006, 2008; *Dunzlaff et al.*, 2010, for a review)

2.11 Cosmic ray modulation

Cosmic rays in the heliosphere experience changes in their intensities as a function of energy, position and time due to the radially out-blowing solar wind and the embedded HMF. This process is known as cosmic ray modulation. When cosmic rays enter the heliosphere, they experience four major modulation processes, namely (1) convection, due to the radially expanding solar wind, (2) energy changes like adiabatic cooling, continuous acceleration like heating or stochastic acceleration and diffusive shock acceleration, (3) diffusion, random walk along and across the turbulent HMF, and (4) drift effects, due to gradient and curvatures in HMF or any abrupt changes in the field direction. These process are discussed in detail in Chapter 3 (see e.g. *Potgieter*, 1984; *Ferreira*, 2002; *Langner*, 2004; *Strauss*, 2010).

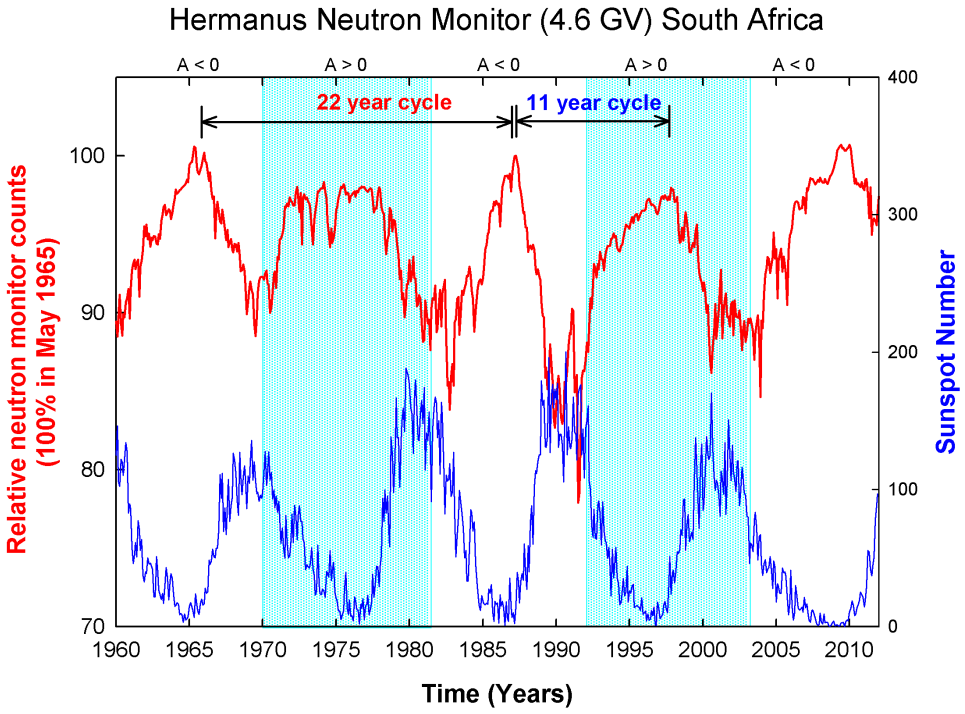

Figure 2.26: The Hermanus cosmic ray neutron monitor count rate (red line) compared to sunspot numbers (blue line). The count rates are normalised to 100% in May 1965. The shaded area represents the $A > 0$ HMF plarity cycle and the $A < 0$ polarity cycle is represented as unshaded area. A 11 year cycle, anti-correlated to the sunspot number cycle, and a 22 year polarity cycle can be seen. Hermanus neutron monitor data from: http://www.nwu.ac.za and yearly sunspot data from: ftp://ftp.ngdc.noaa.gov.

Cosmic ray propagation is determined by solar activity (see Section 2.5) and this leads to a ∼11 year modulation cycle in the cosmic ray intensities. The long-term modulation of cosmic rays as recorded (relative count rates) by the Hermanus neutron monitor with cut-off rigidity ∼4.6 GV is shown in Figure 2.26. The cosmic ray modulation cycle is compared to solar activity indicator; in this case sunspot numbers. From this figure it follows that an anti-correlation exists between the cosmic ray counts and the sunspot number, i.e. cosmic ray count increases with a decrease in sunspot number and vice versa. Also, two long-term cycles are observed, a ∼11 year cycle similar to the sunspot cycle and a ∼22 year cycle as the Hale cycle (discussed in Section 2.5). Understanding this time-dependent cosmic ray modulation is the topic of this work where a numerical modulation model is used to compute cosmic ray intensities over a solar cycle and compare it to various spacecraft observations.

2.12 Spacecraft missions

Spacecraft missions provide crucial data to understand and model the structure, features and properties of the heliosphere and its various constituents. Early missions like the Luna 1 spacecraft launched in 1959 was the first to detect the solar wind as predicted by *Parker* (1958).

Later the first interplanetary mission, the Mariner 2 in 1962 on its way to Venus, confirmed the existence of solar wind and returned the first data about its properties (*Balogh et al.*, 2008). Numerous space missions since then provided us with in-situ observations and helped us to study different aspects like the physical properties and composition of solar wind, the magnetosphere of Earth and other various planets, the Sun, its interior, its atmosphere, energetic particles in the heliosphere, etc.

From a heliospheric perspective, spacecraft missions can be divided into missions which explore the inner heliosphere and missions which explore the outer heliosphere. The spacecraft missions that explore inner heliosphere are considered here as those spacecraft which orbit Earth and orbiting Sun from 0.3 AU to 5.5 AU, which include the IMP series, Helios 1 and 2, ACE, SOHO, STEREO, Ulysses, PAMELA, IBEX etc. The spacecraft missions that have explored the outer heliosphere, towards distant planets and the interstellar space, are Pioneer 10, Pioneer 11, Voyager 1, Voyager 2, Cassini, New Horizon etc. The numerical results obtained by this study are compared with cosmic ray measurements from different spacecraft exploring the inner and outer heliosphere. For this work, cosmic ray observations from the IMP 8, Ulysses, Voyager 1 and Voyager 2 are frequently used. Note that only these spacecraft which are important for this study are now briefly discussed below.

2.12.1 The IMP 8 mission

IMP 8 (International Monitoring Platform) also known by the names Explorer 50 and IMP-J was launched by NASA on the 26th October 1973. IMP 8 was the last in a series of ten proposed IMP missions to observe the Earth and Sun environment, which include the electric and magnetic fields, plasmas, energetic solar particles, anomalous cosmic rays and galactic cosmic rays (*Paularena and King*, 1999).

On-board IMP 8 there are three plasma experiments, a magnetometer and several energetic particle experiments. The experiment on-board IMP 8 which is utilised for this study is CPME (Charged Particle Measurement Experiment). This instrument is a solid state telescope measuring fluxes of protons in 11 energy channels between 0.29 and 440 MeV, and alpha particles in 6 channels between 0.64 and 52 MeV/n. The CPME has two major components, the PET (Proton-Electron Telescope) and five tin-window Geiger-Mueller tubes. The PET instrument measures and identifies the protons (*Paularena and King*, 1999; *Lario et al.*, 2003) which are compared with the numerical model results in this study. In this study the normalised 26-day average counting rates for >70 MeV protons as observed by the PET telescope on the IMP 8 spacecraft is used as 1 AU observations of cosmic ray intensities. The mission was officially terminated by NASA in October 2001 (*Lockwood and Webber*, 1992; *Webber and Lockwood*, 1995; *Richardson et al.*, 2007; *Ahluwalia and Lopate*, 2007).

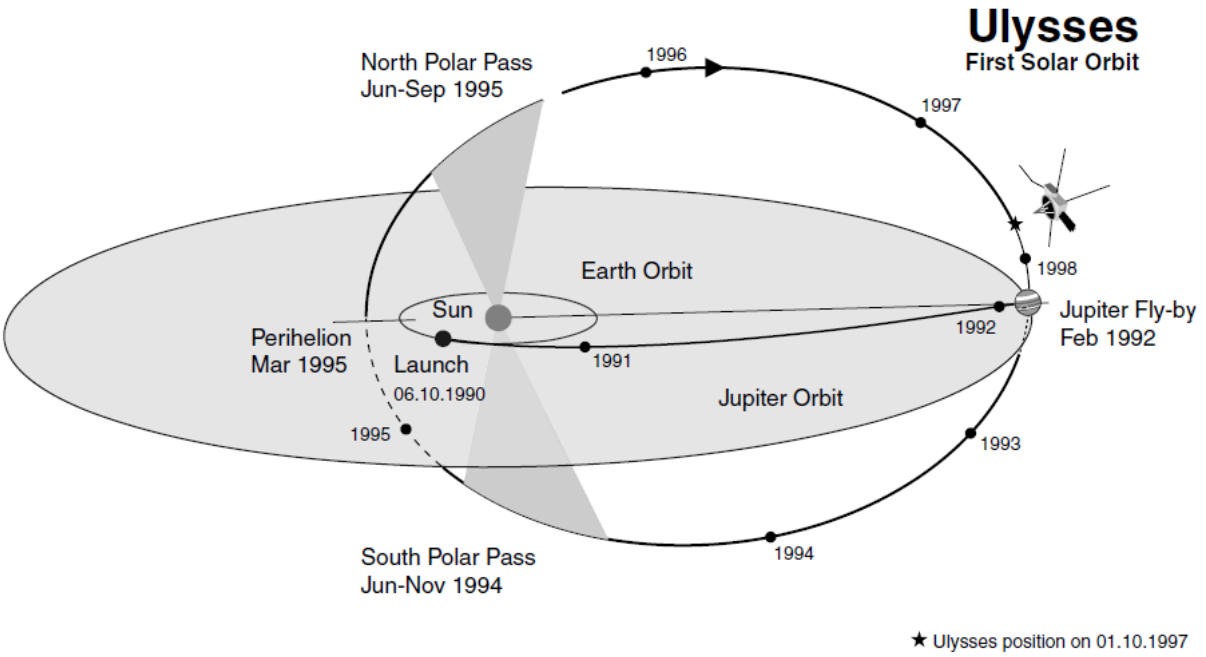

Figure 2.27: The first orbit of Ulysses around the Sun viewed from a perspective of 15^o above the ecliptic plane. The dark shaded wedges represents the period during the polar passes when the spacecraft is above $\pm 70^o$ heliolatitude. The first fast latitude scan occurred from the end of 1994 to about mid-1995. From *Heber and Potgieter* (2006).

2.12.2 The Ulysses mission

Ulysses was the first spacecraft to travel out-of-ecliptic plane to higher heliolatitudes in order to take in-situ measurements of the unexplored regions of the Sun. Ulysses was a joint ESA-NASA mission and was launched on 6th October 1990 during a declining phase of the solar cycle 22. Instruments on-board Ulysses allowed studies of the solar wind plasma including its minor heavy ion constituents, the HMF, solar, planetary and interplanetary energetic particles, galactic cosmic rays and the anomalous cosmic ray component. Since its launch and the Jupiter fly-by on February 1992, the spacecraft is orbiting the Sun in an elliptical orbit at an inclination of 80.2^o to the solar equator (*Wenzel et al.*, 1992; *Marsden*, 2001; *Heber*, 2011).

The orbital period of Ulysses is 6.3 years, aphelion (furthest point to the Sun) is 5.3 AU, perihelion (closest point to the Sun) is 1.3 AU and the radial distance from the Sun is 2.2 AU at maximum latitude. A graphical illustration of the first orbit of Ulysses around the Sun during the period 1992-1998 which as viewed from a perspective of 15^o above the ecliptic plane is shown in Figure 2.27. During this first orbit around the Sun, Ulysses completed its first Fast Latitude Scan (FLS) from the Sun's South pole to North pole i.e. transit between 80^{o}S and 80^{o}N. Both the South polar pass and the North polar pass period is shown as a wedge shaped dark shading in Figure 2.27. Where polar passes are defined to be the periods during which the spacecraft is above 70^o heliolatitude in both hemispheres.

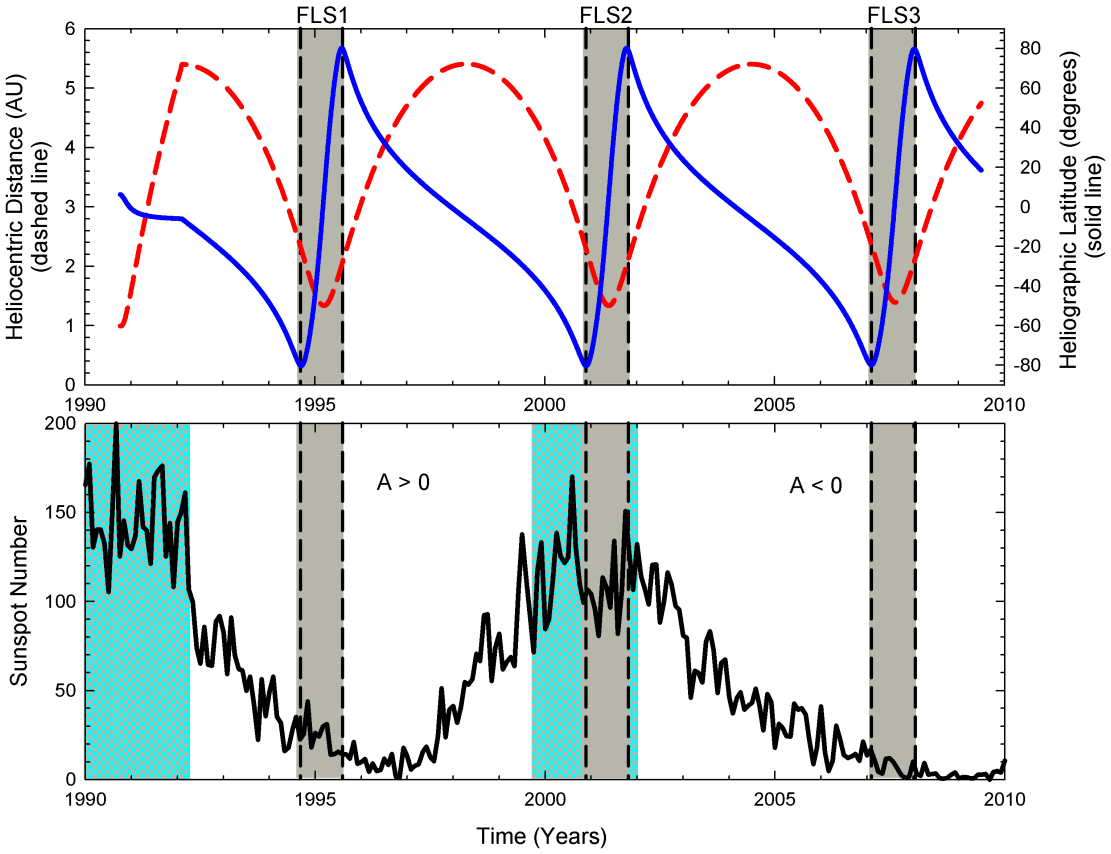

Figure 2.28: The top panel shows the radius and helographic latitude of Ulysses (data from: http://ulysses-ops.jpl.esa.int) during its lifetime. The grey shaded area between the vertical dashed lines on both the top and bottom panel represents the Fast Latitude Scan periods . The first, second and third Fast Latitude Scans are represented as FLS1, FLS2 and FLS3 respectively. The bottom panel shows the observed monthly sunspot numbers (data from: ftp://ftp.ngdc.noaa.gov). The dotted cyan pattern shaded area represents the period where there was not a well defined HMF polarity. Note that the FLS1 took place during a solar minimum period when the HMF polarity was $A > 0$ and the FLS3 took place also during a solar minimum period but for an $A < 0$ HMF polarity cycle. However, FLS2 took place during a solar maximum period when the sunspot number was high and no well defined polarity existed.

Ulysses completed three FLS periods, two during moderate to minimum solar conditions and one during solar maximum. The top panel of Figure 2.28 shows the radius and helographic latitude of Ulysses during its lifetime. The grey shaded area between the two vertical dashed lines on the top and bottom panel represents the Fast Latitude Scan periods, the first, second and third Fast Latitude Scans are represented as FLS1, FLS2 and FLS3 respectively. The bottom panel of the figure shows the observed monthly sunspot numbers which represents the level of solar activity. The dotted cyan pattern shaded area on the bottom panel represents the period where there was not a well defined HMF (HMF) polarity. The FLS1 took place during a solar minimum period of ∼1994.5 to ∼1995.5 when the HMF polarity was $A > 0$ and the FLS3 took place during a solar minimum period of ∼2007 to ∼2008 but when the HMF polarity was $A < 0$. However, FLS2 took place during a solar maximum period from ∼2001 to ∼2002 when

the sunspot number was at a high and without a well-defined polarity (see *Heber and Potgieter*, 2006; *Heber et al.*, 2009; *Heber*, 2011; *Smith*, 2011).

The scientific instruments on-board Ulysses comprised of two magnetometers, two solar-wind plasma instruments, a unified radio/plasma wave instrument, three energetic charged particle instruments covering a wide range of energies and species, an interstellar neutral gas sensor, a solar X-ray/cosmic gamma-ray burst instrument, a cosmic dust sensor and two radio science investigations (*Wenzel et al.*, 1992; *Simpson et al.*, 1992). The Cosmic Rays and Solar Particle Investigation (COSPIN) experiment on-board Ulysses consist of a set of five telescope subsystems. They are High Energy Telescope (HET), Low Energy Telescope (LET), twin Anisotropy Telescopes (ATs), High Flux Telescope (HFT) and Kiel Electron Telescope (KET). The KET aboard Ulysses measure protons and helium in the energy range from 6 MeV/nucleon to above 2 GeV/nucleon and electrons in the energy range from 3 MeV to a few GeV. Among the different particle channels from the KET, the proton channel 0.549-2.43 GV is used for this study. This particle channel roughly corresponds to the same average characteristic rigidity as IMP 8 (discussed above) and will be abbreviated as ∼2.5 GV protons from now onwards (*Simpson et al.*, 1992; *Heber et al.*, 1999a, 2009). The Ulysses mission finally ended its exploration of the heliosphere on the 30th June 2009 after 18.8 years lifetime (*Heber*, 2011; *Smith*, 2011).

2.12.3 The Voyager interstellar mission

The Voyager interstellar mission is a space mission by NASA and managed by the Jet Propulsion Laboratory to explore the solar system beyond the neighbourhood of the outer planets to the outer heliosphere and possibly into the LISM. This mission consists of twin spacecraft Voyager 1 and Voyager 2, probing the northern and southern hemispheres of the heliosphere. Voyager 2 was launched first on August 20, 1977 and later Voyager 1 on September 5, 1977 (*Kohlhase and Penzo*, 1977; *Burlaga and Behannon*, 1982). The primary focus was to explore the planets Jupiter, Saturn and their moons. However, Voyager 2 also went on to explore Uranus and Neptune. At present Voyager 1 is the farthest human made object from the Earth and both spacecraft are still sending scientific information back to NASA's Deep Space Network at Earth.

Figure 2.29 shows the trajectory of both the Voyager 1 and Voyager 2 spacecraft in radial distance (top panel) and polar angle (bottom panel). Note the different radial distance and polar angles between the two spacecraft. This is important for this work when comparing the observed cosmic ray intensities between the two Voyagers. As of January 2012 (the period of the last cosmic ray observations used in this work), Voyager 1 is now beyond 119.26 AU, 34.5 degrees in latitude (polar angle, $\theta = 55.5^o$) and 267.8 degrees in longitude, while Voyager 2 is beyond 97.32 AU, -29.7 degrees in latitude (polar angle, $\theta = 119.7^o$) and 311.1 degrees in longitude (heliographic coordinates). Voyager 1 is escaping the solar system at a speed of about 3.6 AU per year and Voyager 2 is escaping the solar system at a speed of about 3.3 AU per year (*Izmodenov et al.*, 2003).

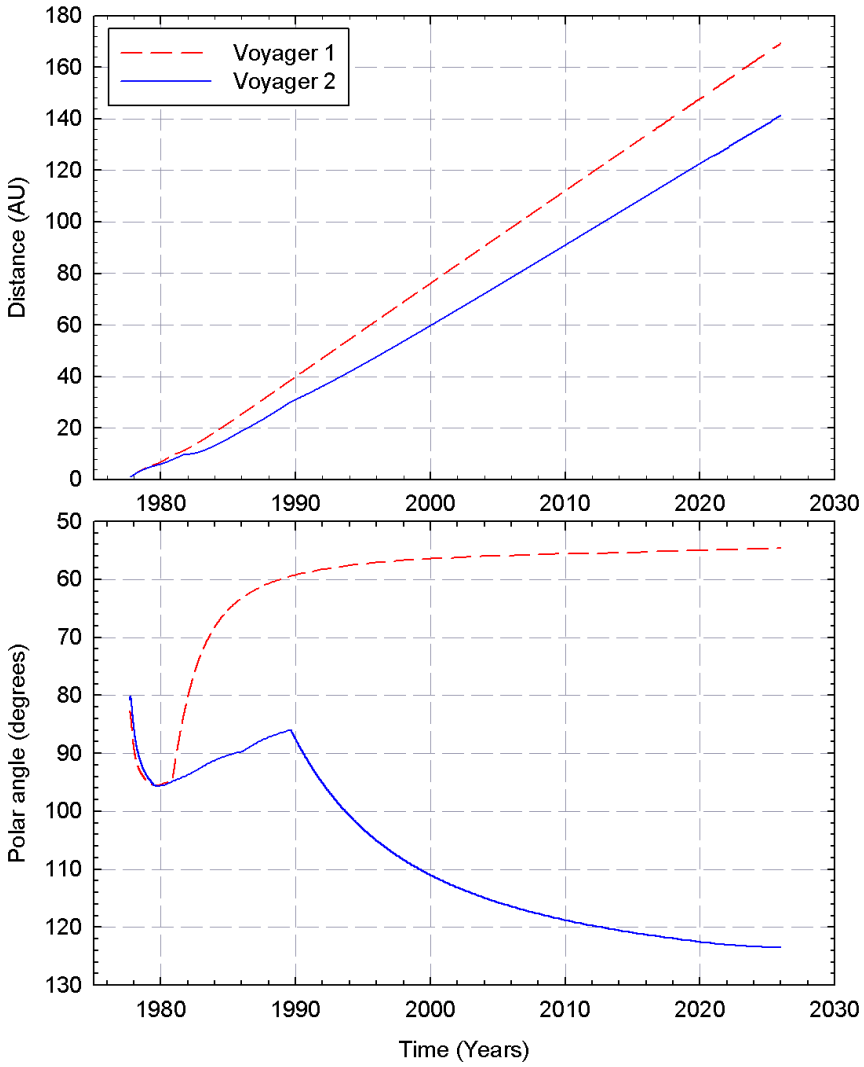

Figure 2.29: The trajectory of the Voyager 1 and Voyager 2 spacecraft in terms of radial distance from the Sun (top panel) and polar angle θ (bottom panel). The equatorial plane is at $\theta = 90^o$. Data from: http://cohoweb.gsfc.nasa.gov.

The scientific investigations on-board both Voyagers are Imaging Science, Infrared Radiation, Photopolarimetry, Ultraviolet Spectroscopy, Radio Science, Cosmic Ray Particles, Low Energy Charged Particles, Magnetic Fields, Planetary Radio Astronomy, Plasma Particles and Plasma Waves (see *Behannon et al.*, 1977; *Bridge et al.*, 1977; *Kohlhase and Penzo*, 1977; *Krimigis et al.*, 1977; *Scarf and Gurnett*, 1977; *Stone et al.*, 1977). Among these, a few instruments are defective and a few were switched off to save energy.

The Cosmic Ray System (CRS) instruments are active on both spacecraft until now, which investigate the energy spectra, isotopic composition of cosmic ray particles and trapped planetary energetic particles. The CRS investigation consist of three telescopes, High Energy Telescope System (HETS), the Low Energy Telescope System (LETS) and the Electron Telescope (TET) (*Stone et al.*, 1977). This study compares the cosmic ray intensities from a numerical model with both Voyager observations from the CRS investigation and is limited to galactic

cosmic ray protons e.g. the 133-242 MeV and >70 MeV measurements (*McDonald et al.*, 1992; *Webber and Lockwood*, 1995, 2001).

Of importance to this work is that the Voyager mission consists of three distinct phases. They are the TS, the heliosheath exploration and the interstellar exploration phases. The passage through the TS by both the Voyager spacecraft ended the TS phase and began the heliosheath exploration phase. Voyager 1 crossed the TS on December 2004 at a distance of 94 AU from the Sun (*Decker et al.*, 2005; *Stone et al.*, 2005) and Voyager 2 crossed at 84 AU in August 2007 in the southern hemisphere, 10 AU closer to the Sun compared to Voyager 1 in the north hemisphere (*Richardson et al.*, 2008; *Stone et al.*, 2008). After passing through the TS both the spacecraft are in the inner heliosheath, the region of shocked solar wind between the TS and the heliopause. Recently, *Krimigis et al.* (2011) reported that Voyager 1 has entered, or very close to the heliopause, a region never been reached by any spacecraft. According to NASA, both Voyagers have enough electrical power and fuel to operate and send back data at least until 2020 (*Gurevitz*, 2005). Therefore, this work also aims to predict future observations along both the Voyager spacecraft.

2.13 Summary

In this chapter the necessary background in order to understand cosmic ray modulation in the heliosphere were given. The discussion started with the Sun, our nearest star which is 1 AU away from Earth, and its properties. The Sun has a differential rotation period, it rotates faster (∼25 days) at the equator and slower (∼36 days) towards the poles. The different regions of the Sun were also discussed which include, the corona the upper-most and the extended plasma atmosphere of the Sun which becomes the solar wind.

Different features observed on the Sun were also discussed. These include: (1) Sunspots, visible dark areas of irregular shape on the solar surface, (2) faculae, which appear as bright areas that are usually most easily seen near the edge of solar disk, (3) granulation, cellular features observed on the solar surface, (4) filaments and prominences, arch like magnetic structures confining a cool and dense plasma, (5) flares, powerful magnetic events in the Sun and (6) coronal mass ejections, huge clouds of plasma that erupt from the Sun's corona.

Sunspots are a measure (proxy) of solar activity. The number of sunspots increases and decreases every ∼11 years forming a ∼11 year solar cycle. The peak of sunspots count is called a solar maximum period and time when few are counted is called a solar minimum period. Also a ∼22 year magnetic cycle is observed, called the Hale cycle, due to the polarity reversal of the Sun's magnetic field which occurs every ∼11 years.

As the solar wind blows radially out from the Sun, it forms the heliosphere, the entire region of space influenced by the Sun and its magnetic field called HMF. The radially expanding hot upper atmosphere of the Sun, the solar wind, carries out the HMF into the interplanetary space

towards the LISM. When the solar wind encounters the LISM, a boundary layer is formed, which separates the solar plasmas from the interstellar plasma, called the heliopause. Due to this encounter, the supersonic solar wind suddenly decreases to a subsonic speed at a shock region called the TS. Both the Voyager spacecraft penetrated through this region, Voyager 1 reached the TS at ∼94 AU and Voyager 2 at ∼84 AU from the Sun. If the LISM has a supersonic speed, the region where this speed decreases to a subsonic speed is called bow shock. The heliosheath is the region between the TS and bow shock where subsonic speed prevails. It is divided into two namely, the inner heliosheath region which are between TS and the heliopause and the outer heliosheath the region between heliopause and the bow shock.

The solar wind can be divided into slow (∼400 km.s^{-1}) and fast (∼800 km.s^{-1}) solar wind. The fast solar wind is evolved from regions where open magnetic fields are found, e.g. from large coronal holes. However, a slow solar wind originates from regions where magnetic field loops obstruct the plasma flow and from small coronal holes and also from the edges of large coronal holes. The solar wind speed possess a latitudinal dependence during solar minimum periods, a fast solar wind is seen near the polar regions and the speed decreases towards the equatorial plane where a slow wind is observed. The latitudinal dependence of the solar wind was confirmed by Ulysses spacecraft observations. However, during solar maximum, Ulysses observed no clear latitudinal dependence in the solar wind speeds but highly variable solar wind speeds were observed. The radial dependence of the solar wind shows that both the fast and slow speed are accelerated within 0.1 AU and becomes a steady flow at around 0.3 AU.

Carried with the solar wind into the heliosphere is the HMF. The basic structure of the HMF used in this work is a Parker spiral (*Parker*, 1958) modified at poles (*Jokipii and Kota*, 1989). The magnitude of the HMF exhibits a ∼11 year cycle correlated with the sunspot cycle. During solar maximum conditions the HMF magnitude increases by a factor of ∼2 when compared to the magnitude for solar minimum conditions.

The HCS is a magnetic boundary structure encircling the Sun. It separates the oppositely directed open magnetic field lines that originate from the solar surface. Since the rotation axis and the magnetic axis of the Sun is tilted by an angle α, as Sun rotates it forms a current sheet which oscillates about the heliographic equator to form a series of peak and valleys which spiral outwards forming HCS. The waviness of the HCS is correlated to the solar activity, during solar maximum periods the tilt increases to $\sim 75^o$ and which in turn increase the waviness of the HCS and during a solar minimum periods the tilt decreases to $\sim 5^o$ thereby decreasing the waviness. The HCS has a significant effect on cosmic ray transport, where it effect the drift motions of the cosmic rays.

Cosmic rays are energetic charged particles which can be classified mainly into four types depending on their origin. They are (1) galactic cosmic rays, which come from outside the heliosphere, probably accelerated by shock waves in the galaxy, (2) solar energetic particles, those particles of solar origin which are accelerated by solar flares, coronal mass ejection and shocks in interplanetary medium, (3) anomalous cosmic rays, originally interstellar neutral

atoms which got ionised and accelerated inside the heliosphere and (4) Jovian electrons, the energetic electrons emitted into the interplanetary space by Jupiter's magnetosphere. For this study galactic cosmic rays are considered, especially to understand the physics behind the $\sim$11 year and $\sim$22 year cosmic ray cycles. The spacecraft missions relevant to this study, IMP 8, Ulysses and Voyager missions were also discussed. In the next chapter, an overview of the cosmic ray transport in the heliosphere is given.